

Chapter 2

Brief Review on Integrated Planar Waveguide-Based Optical Sensor

Aradhana Dutta

Abstract Planar optical waveguides are the input devices to build an integrated optical sensor. This chapter provides review made in the recent advancement of integrated optical sensor that involves guided light with substantial developments made at a very rapid pace. The basic concept and equations of electromagnetic (EM) wave theory requisite for lightwave propagation in optical waveguides are presented. The light confinement and formation of modes in the waveguide are qualitatively explained, considering a slab waveguide. Maxwell's equations, boundary conditions, are described as they form the basis for the following chapters. Theoretical consideration and supportive calculation to understand the basic properties of optical waveguide is presented for a step-index waveguide. Further, the derivation of dispersion equations is explained in detail in order to understand the dispersion characteristics of optical waveguide. Rigorous three-dimensional analysis usually requires numerical calculations, and therefore, this chapter presents several methods such as finite element method, finite difference time domain, and beam propagation method necessary for mode analysis of optical waveguide. The detection of glucose level in blood is a highly researched area in the quest for a sensor that can give accurate measurements, in short time, with minimum invasiveness. Although several optical techniques are being explored for glucose detection including infrared spectroscopy however, there are limitations to these techniques and involve complications. A short review is done on available medical and engineering concepts and attempt is made to discuss how far these can be applied to optical waveguide-based sensor with fine accuracy and high sensitivity.

Keywords Planar optical • Optical waveguide • Waveguide sensor • Waveguide modes • Mode analysis • Electromagnetic wave • Dispersion equation

2.1 Introduction

Following the introduction chapter, this chapter presents the important concepts and significant achievements in the area of optical sensor. We have seen in the introductory chapter that recently, optical techniques have been demonstrated for

sensing applications due to its high sensitivity, selectivity, and low detection time. Such sensing that makes use of change of light energy through bio/chemical/mechanical processes into a detectable signal adds to intrinsic advantages because of its accuracy. As compared to other existing sensing technologies, the strength and versatility of optical sensors lie in the wide range of optical properties that serve to generate the sensing signal. These properties include, but are not limited to refractive index, optical absorption, fluorescence, polarization, and even nonlinear optical processes such as lasing, Raman scattering, and multi-photon absorption and emission. When used alone or in combination, the sensing signals can provide vast amount of information regarding the presence and interaction of bio- and chemical molecules. As a result, optical sensors have broad applications in clinical diagnostics, biotechnology industry, pharmaceuticals, and petroleum adulteration. In this direction, waveguide optics has become attractive for sensing application that includes the following:

1. High sensitivity.
2. Imperviousness to any type of electromagnetic interference (E.I).
3. Small size, light weight, and great suppleness.
4. Capability of resisting to chemically belligerent environments.
5. Easy interface with fiber optic network.
6. Low detection time

For performance evaluation of an optical sensor, there are three basic characteristics, namely

- (i) Light–analyte interaction;
- (ii) Sensor miniaturization; and
- (iii) Incorporation of fluidics with optical sensing elements.

Initially we have started this chapter with the fundamentals of optical waveguide, as its principle forms the basis for optical sensing mechanism. We have described different types of optical sensors such as fiber optic sensor and planar waveguide sensor. Since the sensor developed has been used for detecting adulteration in this regard, an assessment has also been done on sensors used for detecting adulteration using waveguide sensors. Finally, we have described works on sensors used for detection of glucose level in blood, as reported by earlier authors from the relevant literature survey as the proposed sensors have been used for detection of glucose level in blood as described in Chap. 6 of this book.

2.2 Fundamentals of Optical Waveguide

Planar waveguides are optical structures that confine optical radiation along the direction of propagation [1]. Considering the refractive index distribution in the planar waveguide structure, these can be classified as step-index waveguides or

graded index waveguides. The step-index planar waveguide is formed by a uniform planar film with a constant refractive index (homogeneous film, $n_f = \text{constant}$), surrounded by two dielectric media of lower refractive indices [2]. The homogeneous upper medium has a refractive index of n_c , and the lower medium, with refractive index n_s , is often called substrate. Usually, it is assumed that the refractive index of the cover is less than or equal to the refractive index of the substrate, $n_c \leq n_s$, and in this way, we have $n_f < n_s \leq n_c$.

If the upper and the lower media have equal optical constants, then the structure forms a symmetric planar waveguide, whereas if the upper and lower media are different, then it is known as an asymmetric planar waveguide (Fig. 2.1). If the high-index film is not homogeneous, but its refractive index is depth-(thickness of the waveguide) dependent (along the x -axis in Fig. 2.2), the structure is called a graded index planar waveguide [3]. Usually the refractive index is maximum at the top surface, and its value decreases with thickness until it reaches the value corresponding to the refractive index of the substrate (Fig. 2.2).

Asymmetric step-index planar waveguides are fabricated by depositing a high-index film on top of a lower index substrate, by means of physical methods

Fig. 2.1 Asymmetric step-index planar waveguide. Right refractive index profile, where $n_f < n_s \leq n_c$

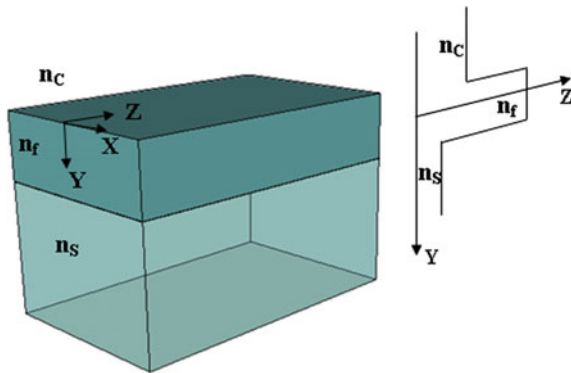
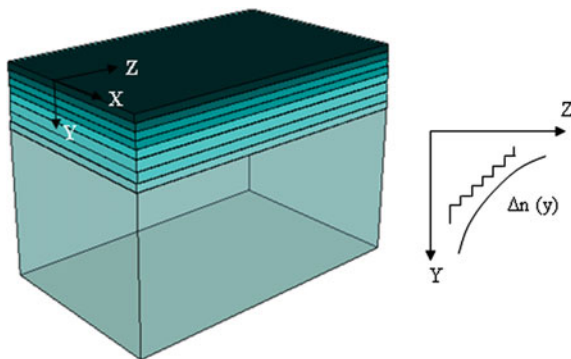


Fig. 2.2 Graded index planar waveguide



(thermal evaporation, molecular beam epitaxy, sputtering, etc.) or chemical methods (chemical vapor deposition, metal-organic chemical vapor deposition, etc.).

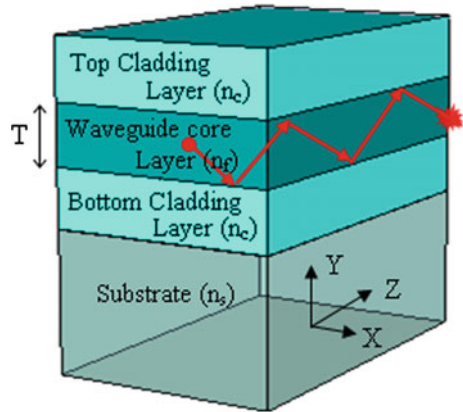
The more accurate description of light propagation within a waveguide is obtained by means of Maxwell's equations. When the geometric boundary conditions at media interfaces are introduced, only discrete solutions of the wave equations are permitted. This means that only discrete waves can propagate, namely 'modes,' characterized by discrete amplitudes and discrete velocities [4, 5]. Waveguides can be single-mode or multimode according to whether a single or a multiplicity of modes can propagate. Once the materials constituting the waveguide are set for a given wavelength, the number of supported modes depends on waveguide dimension, namely on the fiber core radius or the planar waveguide thickness. A trait of a guided mode which is predominantly essential for sensing devices is its spatial amplitude distribution. Often, in fact, the interaction between the propagating mode and the quantity to be measured (the measurand) occurs through the evanescent field of the mode itself, namely its exponentially decreasing tail.

2.2.1 Wave Equation in Symmetric Slab Waveguide

Figure 2.3 shows the schematic view of a symmetric waveguide consisting of a waveguide layer of refractive index n_f having lightwave confined, top and bottom cladding layers each having of refractive indices n_c , respectively. The wave propagation of the waveguide (Fig. 2.3) can be analyzed considering the Maxwell equation [4, 5] as follows:

$$\nabla \times E = -\mu_0 \frac{\partial H}{\partial t} \quad (2.1)$$

Fig. 2.3 Schematic view of integrated optic waveguide sensor structure



and

$$\nabla \times H = \epsilon_0 n^2 \frac{\partial E}{\partial t} \quad (2.2)$$

where n is the refractive index. Also the plane-wave propagation can be defined as:

$$E = E(x, y) e^{j(\omega t - \beta z)} \quad (2.3)$$

$$H = H(x, y) e^{j(\omega t - \beta z)} \quad (2.4)$$

Substituting Eqs. (2.3) and (2.4) into Eqs. (2.1) and (2.2), we obtain the following two sets of equations for the electromagnetic field components:

$$\begin{cases} \frac{\partial E_z}{\partial y} + j\beta E_y = -j\omega\mu_0 H_x \\ -j\beta E_x - \frac{\partial E_z}{\partial x} = -j\omega\mu_0 H_y \\ \frac{\partial E_y}{\partial x} - \frac{\partial E_x}{\partial y} = -j\omega\mu_0 H_z \end{cases} \quad (2.5)$$

$$\begin{cases} \frac{\partial H_z}{\partial y} + j\beta H_y = j\omega\epsilon_0 n^2 E_x \\ -j\beta H_y - \frac{\partial H_z}{\partial x} = j\omega\epsilon_0 n^2 E_y \\ \frac{\partial H_y}{\partial x} - \frac{\partial H_x}{\partial y} = j\omega\epsilon_0 n^2 E_z \end{cases} \quad (2.6)$$

From Fig. 2.3, it is observed that both the electromagnetic fields, electric field (E) and magnetic field (H), are y -axis independent, i.e., $\frac{\partial E}{\partial y} = 0$ and $\frac{\partial H}{\partial y} = 0$. Substituting these relations into Eqs. (2.5) and (2.6), two independent electromagnetic modes are obtained, which are denoted as TE mode and TM mode, respectively. The TE mode satisfies the following wave equation:

$$\frac{d^2 E_y}{dx^2} + (k^2 n^2 - \beta^2) E_y = 0 \quad (2.7)$$

where

$$H_x = \frac{-\beta}{\omega\mu_0} E_y \quad (2.8)$$

$$H_z = \frac{j}{\omega\mu_0} \frac{dE_y}{dx} \quad (2.9)$$

and

$$E_x = E_z = H_y = 0 \quad (2.10)$$

From the Eqs. (2.8–2.10), it is seen that the tangential components E_y and H_z should be continuous at the boundaries of two different media and the electric field component along the z -axis is zero (i.e., $E_z = 0$). Since the electric field lies in the plane that is perpendicular to the z -axis, this electromagnetic field distribution is called transverse electric (TE) mode.

Equation (2.6) can be written by considering y independency for TM mode which satisfies the following wave equation:

$$\frac{d}{dx} \left(\frac{1}{n^2} \frac{dH_y}{dx} \right) + \left(k^2 - \frac{\beta^2}{n^2} \right) H_y = 0 \quad (2.11)$$

$$\text{where } E_x = \frac{\beta}{\omega \epsilon_0 n^2} H_y \quad (2.12)$$

$$E_z = -\frac{j}{\omega \epsilon_0 n^2} \frac{dH_y}{dx} \quad (2.13)$$

$$E_y = H_x = H_z = 0 \quad (2.14)$$

Thus, Eq. (2.14) gives the magnetic field component along the z -axis is zero (i.e., $H_z = 0$). Since the magnetic field lies in the plane that is perpendicular to the z -axis, this electromagnetic field distribution is called transverse magnetic (TM) mode. The solution in the case of light propagation with TM polarization is basically the same for the TE polarization, with the exception that the boundary conditions are slightly different, because of the factor $(1/n^2)$ in the continuity of the magnetic field component derivative.

2.2.2 Planar Waveguides and the Modes

Light propagation in the optical waveguide has been analyzed by examining the case of an asymmetric planar waveguide from the point of view of ray optics.

We consider the planar waveguide depicted in Fig. 2.3, where we have assumed that the refractive index of the film n_f is higher than the refractive index corresponding to the substrate n_s and the upper cover n_c . In addition, we assume the usual situation in which the relation $n_s > n_c$ is fulfilled. In this way, the critical

angles that define total internal reflection (TIR) for the cover–film interface (θ_{1C}) and the film–substrate boundary (θ_{2C}) are determined by:

$$\theta_{1c} = \sin^{-1}\left(\frac{n_c}{n_f}\right) \quad (2.15)$$

$$\theta_{2c} = \sin^{-1}\left(\frac{n_s}{n_f}\right) \quad (2.16)$$

In addition, as we have $n_f > n_s > n_c$, it follows that the critical angles fulfill the relation $\theta_{2C} > \theta_{1C}$. If now we fix our attention to the propagating angle θ of the light inside the film (Fig. 2.4), three situations can be distinguished:

- (i) $\theta < \theta_{1C}$. In this case, if the ray propagates with internal angles θ lower than the critical angle corresponding to the film–cover interface θ_{1C} , the light penetrates the cover, as well as the substrate, because $\theta_{2C} > \theta_{1C}$. Thus, the radiation is not confined to the film, but travels in the three regions. This situation corresponds to radiation modes, because the light radiates to the cover layer and the substrate (Fig. 2.5).
- (ii) $\theta_{1c} < \theta < \theta_{2c}$. Light traveling in these circumstances is totally reflected at the film–cover interface; thus, it cannot penetrate the cover region. Nevertheless, the radiation can still penetrate the substrate, and therefore, it corresponds to substrate radiation modes, or in short, substrate modes (Fig. 2.6).
- (iii) $\theta_{2c} < \theta < \frac{\pi}{2}$. In this situation, the ray will suffer total internal reflection (TIR) at the upper and lower interfaces, and thus, the radiation is totally confined and cannot escape the film. This corresponds to a guided mode (Fig. 2.7).

Fig. 2.4 Asymmetric planar waveguide and zigzag trajectory of a ray inside the film

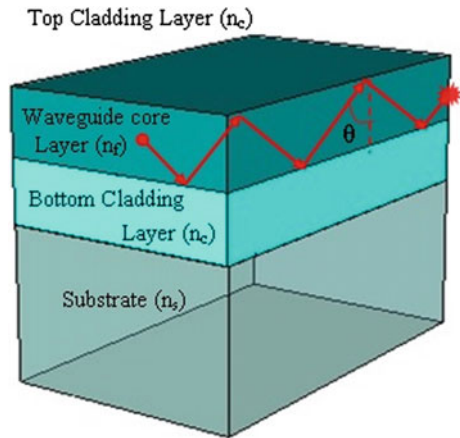


Fig. 2.5 Radiation mode in an asymmetric step-index planar waveguide

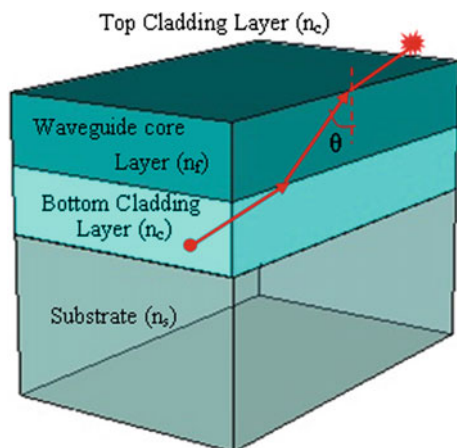


Fig. 2.6 Ray path followed by a substrate radiation mode

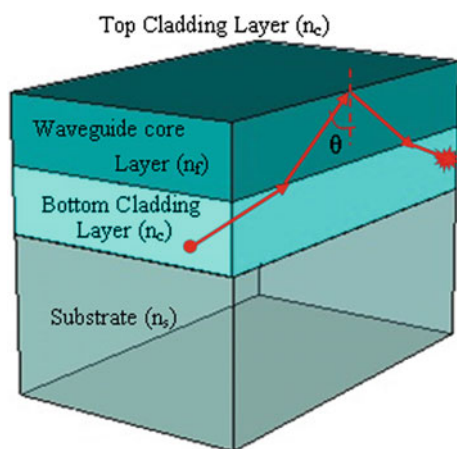
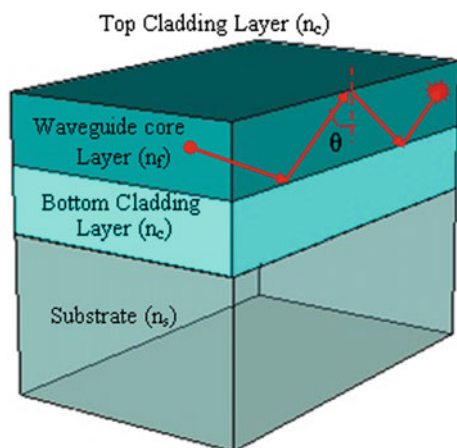


Fig. 2.7 Guided mode in an asymmetric planar waveguide, showing the ray path



The general solution of the wave equation discussed in the previous section has been applied to the case of guided modes supported by asymmetric step-index planar waveguides.

2.2.2.1 Guided Modes

The general solution discussed in the previous Sect. 2.2.1 can easily be applied to the case of guided modes supported by asymmetric step-index planar waveguides, considering the geometry as shown in Fig. 2.8. The three media have refractive indices such as n_c (cover), n_f (film), and n_s (substrate) and are separated by planar boundaries perpendicular to the x -axis, the light propagation being along the z -axis. We further assume that $n_f > n_s > n_c$ and that the plane $x = 0$ corresponds to the cover–film boundary. Therefore, if the film thickness is d , then the film–substrate interface is located at the plane $x = -d$, respectively.

Guided TE Modes

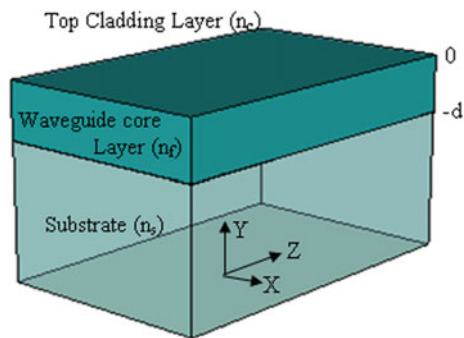
Although step-index planar waveguides are the structures inherently inhomogeneous, within each of the three regions the refractive indices are constant. Thus, considering each region separately, the wave equation for TE modes is expressed as shown in Eq. (2.7).

The propagation constant β associated with a particular mode must fulfill the following condition:

$$k_0 n_s < \beta < k_0 n_f \quad (2.17)$$

Further, the effective refractive index, N , of the guided mode must lie in-between the refractive index of the film n_f and the refractive of the substrate n_s (reference to Fig. 2.8).

Fig. 2.8 Geometry used for the analysis of propagating modes in an asymmetric step-index planar waveguide



$$n_s < N < n_f \quad (2.18)$$

The wave Eq. (2.7) in each homogeneous region can be written as:

$$\frac{d^2 E_y}{dx^2} - \gamma_c^2 E_y = 0 \quad x \geq 0 \quad (\text{Cover}) \quad (2.19)$$

$$\frac{d^2 E_y}{dx^2} + K_f^2 E_y = 0 \quad 0 > x > -d \quad (\text{Film}) \quad (2.20)$$

$$\frac{d^2 E_y}{dx^2} - \gamma_s^2 E_y = 0 \quad x \leq -d \quad (\text{Substrate}) \quad (2.21)$$

where the three parameters γ_c , K_f , and γ_s are given by:

$$\gamma_c^2 = \beta^2 - k_0^2 n_c^2 \quad (2.22)$$

$$K_f^2 = k_0^2 n_f^2 - \beta^2 \quad (2.23)$$

$$\gamma_s^2 = \beta^2 - k_0^2 n_s^2 \quad (2.24)$$

By solving the differential Eqs. (2.22–2.24), the electric fields in the cover, film, and substrate regions can be expressed as:

$$E_y = \begin{cases} Ae^{-\gamma_c x} & x \geq 0 \\ Be^{iK_f x} + Ce^{iK_f x} & -d < x < 0 \\ De^{\gamma_s x} & x \leq -d \end{cases} \quad (2.25)$$

The boundary conditions require that E_y and dE_y/dx must be continuous at the cover–film interface ($x = 0$) and at the film–substrate frontier ($x = -d$), giving place to four equations that relate the constant parameters A , B , C , and D and the propagation constant β . Therefore, we have five unknown quantities to be determined from only a set of four equations. Indeed, one of the constant parameters cannot be determined and should remain free (for instance, the parameter A), and it will be determined once the energy carried by the propagating mode is settled. By solving this set of equations, and after cumbersome calculation, the following equation is obtained:

$$\tan(K_f d + m\pi) = \frac{\frac{\gamma_c}{K_f} + \frac{\gamma_s}{K_f}}{1 - \left(\frac{\gamma_c}{K_f}\right)\left(\frac{\gamma_s}{K_f}\right)}; \text{ where } m = 0, 1, 2, 3, \dots \quad (2.26)$$

This relation is considered as the dispersion relation for the asymmetric step-index planar waveguide and is a transcendental equation involving the parameters that define the waveguide structure (n_c , n_f , n_s , and d), the working wavelength (λ), and the

propagation constant β of the guided mode, and from which one can calculate numerically the propagation constant β . In general, there exist several solutions for the propagation constant β depending on the integer number m . This integer number m is called the mode order, and the associated propagation constant is referred as β_m .

It is convenient to define a set of parameters, called *normalized parameters*, in such a way that the transcendental Eq. (2.26) can be universalized for any asymmetric step-index waveguide. These parameters are defined as:

$$b = (N^2 - n_s^2) / (n_f^2 - n_s^2) \quad (2.27)$$

$$V = k_0 d (n_f^2 - n_s^2)^{1/2} \quad (2.28)$$

$$a = (n_s^2 - n_c^2) / (n_f^2 - n_s^2) \quad (2.29)$$

$$\tan \left[V \sqrt{1-b} \right] = \frac{\sqrt{\frac{b}{1-b}} + \sqrt{\frac{b+a}{1-b}}}{1 - \frac{\sqrt{b(b+a)}}{1-b}} \quad (2.30)$$

In general, Eqs. (2.26) and (2.30) admit a finite number of solutions for a finite number of the integer, m , and thus, the waveguide will support a finite number of guided modes. In this case, we refer to it as a multimode waveguide. In the particular case in which the dispersion equation only admits a solution for $m = 0$, the waveguide is called a monomode or single-mode waveguide.

Guided TM Modes

In this case, we are interested in the determination of the electromagnetic field structure within the planar waveguide based on the magnetic field, because in TM polarization the magnetic field has a single component (H_y). The wave equation for TM propagation in a homogeneous region can be expressed as:

$$\frac{d^2 H_y}{dx^2} + [k^2 n^2 - \beta^2] H_y = 0 \quad (2.31)$$

Following a similar procedure to that performed for TE modes in Sect. 2.2.2.1, a transcendental equation for confined TM waveguide modes in terms of the normalized parameters is obtained as:

$$\tan \left[V \sqrt{1-b} \right] = \frac{\frac{1}{\gamma_1} \sqrt{\frac{b}{1-b}} + \frac{1}{\gamma_2} \sqrt{\frac{b+a}{1-b}}}{1 - \frac{1}{\gamma_1 \gamma_2} \frac{\sqrt{b(b+a)}}{(1-b)}} \quad (2.32)$$

This is the dispersion relation for TM-guided modes of an asymmetric step-index planar waveguides. In this equation, we have defined (say, for simplicity) the parameters as

$$\gamma_1 \equiv \left(\frac{n_s}{n_f}\right)^2, \gamma_2 \equiv \left(\frac{n_c}{n_f}\right)^2 = \gamma_1 - a(1 - \gamma_1)$$

Cut-off

An important aspect concerning waveguides is to know what should be the minimum film width necessary for the waveguide support of a specific mode of order m , at a given wavelength. In this situation, the effective refractive index of this particular mode N should be very close to the substrate refractive index n_s , as it is shown schematically in Fig. 2.9.

In this case, it yields the following:

$$N \approx n_s \Rightarrow b = (N^2 - n_s^2)/(n_f^2 - n_s^2) \approx 0 \quad (2.33)$$

The normalized film thickness V for TE and TM modes at the cutoff is given by

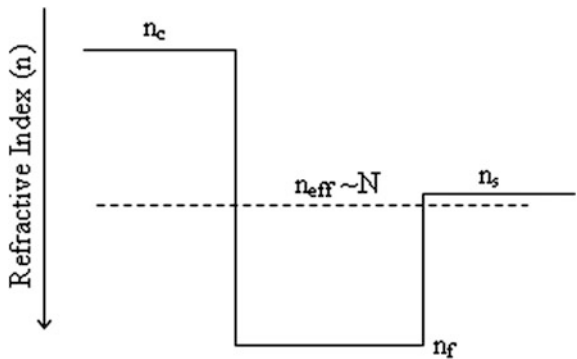
$$V_C^{\text{TE}} = \tan^{-1}(a^{1/2}) + m\pi; \text{ TE modes} \quad (2.34)$$

$$V_C^{\text{TM}} = \tan^{-1}\left(\frac{a^{1/2}}{\gamma_2}\right) + m\pi; \text{ TM modes} \quad (2.35)$$

From these relations, two important conclusions can be deduced:

- (i) As n_c must be lower than n_f , it follows that $\gamma_2 = \left(\frac{n_c}{n_f}\right)^2 < 1$, and consequently it holds that $V_C^{\text{TM}} > V_C^{\text{TE}}$. This inequality implies that if a waveguide supports a

Fig. 2.9 Position of the effective refractive index N , relative to the refractive indices of the waveguide structure, for a mode close to the cutoff



TM mode of m -th order, the waveguide also supports a TE mode of the same order. The reciprocal situation does not apply in general.

- (ii) For a symmetric waveguide ($a = 0$), Eqs. (2.30) and (2.32) yield $V_C^{\text{TM}} = V_C^{\text{TE}} = m\pi$. This indicates that a symmetric planar waveguide always supports at least the fundamental mode $m = 0$, both TE and TM polarized modes, regardless of the size (film thickness) or refractive indices of the guiding structure.

2.2.2.2 Radiation and Leaky Modes

Up to now we have examined the solution of the wave equation for planar waveguides in terms of guided modes, where the radiation is mainly confined only within the film, in the form of evanescent waves. In this case, the mode effective index was restricted between the refractive index of the film and that of the substrate. Nevertheless, the wave equation, for both TE and TM polarization light, also admits solutions for effective indices lower than n_s . In this case, we are dealing with radiation modes, where the light is no longer confined to the film, but can ‘leak’ to adjacent regions, losing the light power inside the film core as the wave propagates along the waveguide. For this reason, these types of solutions are often called leaky modes.

For effective refractive index values lower than n_s and higher than n_c (i.e., $n_c < N < n_s$ or $k_0 n_c < \beta < k_0 n_s$), the solutions in the film and substrate regions are in the form of oscillatory functions, while the behavior of the fields in the cover region is in the form of exponential decay. This condition $\beta < k_0 n_s$ corresponds to substrate radiation modes, where the light is not only confined to the film region, but also spreads out to the substrate. In addition, the solutions for these leaky substrate modes are not discrete, but instead the wave equation for substrate modes admits an infinite number of solutions for continuous propagation constant values β (or effective refractive index N). Finally, if the modal effective refractive index N is lower than n_c ($N < n_c \Rightarrow \beta < k_0 n_c$) the solution for the modal fields in the three regions is in the form of sinusoidal functions. In this case, the field pattern corresponds to a radiation mode, where the light cannot be confined in the film but leaks to the cover and substrate regions. Also, as in the case of substrate modes, there exist a continuous and infinite number of values for the propagation constant of radiation modes, with an infinite number of solutions for the electromagnetic field distribution.

2.2.3 Introduction to Numerical Methods for Approximate Modal Analysis

There are several numerical methods for modal characterization in optical waveguides which yield good results in general. However, we will describe here four widely used methods.

2.2.3.1 Effective Index Method (EIM)

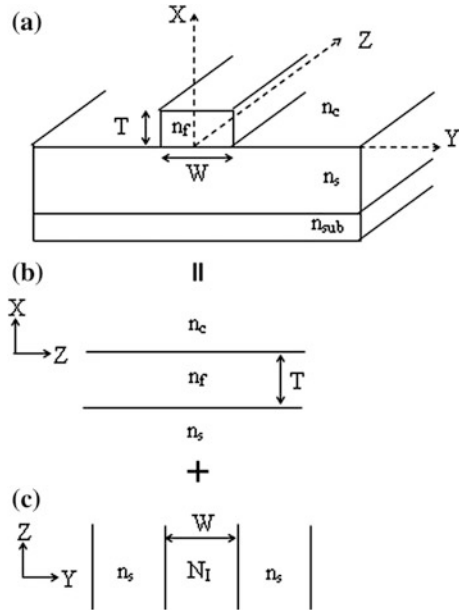
Marcatili's method [6] was extended by Knox and Toullos [7] who proposed the effective index method (EIM), which soon after became one of the most popular methods for the analysis of optical waveguides. Unlike numerical methods, EIM is considered as semi-analytical methods, which make certain approximation to the structure under consideration and then solve the resulting simplified problem analytically. The popularity of the EI method is due to its simplicity, which comes from the fact that it reduces the three-dimensional wave guide structures into an equivalent two-dimensional structure.

This method is one of the simplest approximate methods for obtaining the modal fields and the propagation constant analysis for calculating the propagation modes of channel waveguides. It applies the tools developed for planar waveguides to solve the problem of two-dimensional (2D) structures in channel waveguides having arbitrary geometry and index profiles. It consists of solving the problem in one dimension, described by the x coordinate, in such a way that the other coordinate (the y -coordinate) acts as a parameter. In this way, one obtains a y -dependent effective index profile; this generated index profile is treated once again as a one-dimensional problem from which the effective index of the propagating mode is finally obtained. The propagation constants supported by a 2D channel waveguide having a refractive index profile which depends on two coordinates $n = n(x, y)$ are then calculated by solving the propagation modes for two 1D planar waveguides. The EIM treats the channel waveguide as the superimposition of two 1D waveguides: planar waveguide-I confines light in the x -direction, while planar waveguide-II traps light in the y -direction (as shown in Fig. 2.10). For propagating, modes polarized mainly along the x -direction (E_x^{pq}), where the major field components are E_x , H_y and E_z . The propagation of these polarized modes is similar to the TM modes in a 1D planar waveguide, and their solutions will correspond to the effective indices N_1 . Further, the second planar waveguide (waveguide-II) is considered to be built from a guiding film of refractive index N_1 , which has previously been calculated. The modes for the second planar waveguide are TE polarized, with E_x , H_y and H_z as nonvanishing components, because the light is mainly polarized along the x -direction.

In Fig. 2.10, an analytical model of simple effective index method (SEIM) for three-dimensional (3D) waveguide geometry has been shown, where

Fig. 2.10 Analytical model of effective index method for 3D waveguide geometry.

a 3D waveguide-I **b** 2D waveguide-I **c** 2D waveguide-II



- N_I = Effective refractive index of 2D waveguide-I
 $n_s = n_c$ = Refractive index of upper cladding and lower cladding
 n_{sub} = Refractive index of substrate
 T = Thickness of 2D waveguide-I and
 W = Width of 2D waveguide-II

The procedure for the calculation of effective refractive index for 3D waveguide geometry can be summed up as follows [8]:

1. The two-dimensional optical waveguide is replaced with a combination of two one-dimensional optical waveguides.
2. For each one-dimensional waveguide, the effective index is calculated along y -axis.
3. The waveguide is modeled by using the effective index calculated in step (2) along x -axis.
4. The effective index is to be obtained by solving the model in step-3 along x -axis.

In the analysis of optical waveguides, analytical methods such as effective index method (EIM) and Marcattili's methods are slightly less accurate than finite difference time domain (FDTD) and beam propagation method (BPM) [9]. In spite of the lower accuracy, these methods have become popular waveguide design tools because of their simplicity, easier to use, and require lesser numerical calculations. The ability to convert a three-dimensional problem into two-dimensional one is the main feature and advantage of this method [8]. So we tried to use this method in the study of mode propagation of our proposed planar waveguide-based optical sensor in the proceeding chapters of this book.

2.2.3.2 Finite Element Method (FEM)

Finite element method (FEM) uses a variational formulation for the solution of waveguide problems [9]. For dielectric waveguides, the usual approach is to use all three components of the H or the E vector. The advantage of using the three components of the field is that no boundary conditions need to be set except at the exterior boundary. From Maxwell's equations,

$$\nabla \times \epsilon_r^{-1}(\nabla \times H) = k_0^2 H \quad (2.36)$$

Taking the inner product of this equation with H^* leads to a functional of the form

$$F = \int_S [(\nabla \times H)^* \cdot \epsilon_r^{-1}(\nabla \times H) - k_0^2 H \cdot H^*] dx dy \quad (2.37)$$

If the trial function coefficients are a_i , then requiring $\partial F / \partial a_i = 0$ provides the equations for the matrix eigenvalue problem. The trial functions must span the whole domain and satisfy the exterior boundary conditions, and this becomes difficult for arbitrary shapes. Thus, the finite element method discretizes the domain into a set of adjoining triangles, and the trial functions are defined within each triangle with unknown coefficients. In the nodal element scheme, the trial functions are expressed in the nonorthogonal area coordinates ζ_i , and linear higher-order trial functions in terms of the ζ_i can be used. Further, the integrations of the functional can be performed for each triangle before the matrix equation is assembled. The problem with the functional in Eq. (2.37) is that, spurious eigenvalue modal solutions occur. Furthermore, the formulation requires that β be specified, and the corresponding frequency ω in k_0 is obtained. Since the divergence equation has not been specifically set in this functional, inclusion of this equation in the functional with a summation parameter α mitigates this. While this approach does not eliminate the spurious modes, it pushes them to the higher-order modes depending on the choice of α . Some check needs to be made to ensure that the spurious modes are eliminated from the solutions by running the code with different values of α . Using this technique, Rahman and Davies [10] have obtained results on a ridge guide that remains the benchmark against which all other methods are compared. This method has also been used by other groups [11] for modal solutions. An improvement on the three-component field method was suggested by Cendes [12], in which the transverse fields are defined by edge elements and the longitudinal field is defined by the usual nodal elements. An edge element between the triangle vertices is defined by,

$$W_{ij} = (\zeta_i \nabla \zeta_j - \zeta_j \nabla \zeta_i) \quad l_{ij} \quad (2.38)$$

where ζ_i is the area coordinate defined above and l_{ij} is the length of the edge between these vertices.

The result of this definition is that the edge element is a trial function that is along the edge ij . The functional used here is given in Eq. (2.38), and the preferred field set is the components of E . With this choice of trial functions, the spurious modes are eliminated. Use of second-order edge elements has given excellent results. Recent work in the finite element area has focused on the use of edge elements.

2.2.3.3 Finite Difference Time Domain (FDTD) Method

The FDTD technique represents a widely used propagation solution technique in integrated optics, especially in photonic band gap device computations where the beam propagation solutions are inadequate or cannot cope with the geometry. The major limitation is that the three-dimensional version requires large storage and extremely long computation times. The basic technique has been outlined in several papers and books devoted to the technique, for example, [13] and [14]. The solution of the wave propagation is by direct integration in the time domain of the Maxwell curl equations in discretized form. For example, the component of the curl equation is given by,

$$\frac{\partial H_y}{\partial x} - \frac{\partial H_x}{\partial y} = \frac{\partial D_z}{\partial t} \quad (2.39)$$

Discretizing via central differences in time and space gives the following:

$$\begin{aligned} & \varepsilon \left[\frac{E_z^{t+\Delta t}(x, y, z) - E_z^t(x, y, z)}{\Delta t} \right] \\ &= \left[\frac{H_y^{t+\Delta t/2}(x + \Delta x/2, y, z) - H_y^{t+\Delta t/2}(x - \Delta x/2, y, z)}{\Delta x} \right] \\ & \quad - \left[\frac{H_x^{t+\Delta t/2}(x, y + \Delta y/2, z) - H_x^{t+\Delta t/2}(x, y - \Delta y/2, z)}{\Delta y} \right] \end{aligned} \quad (2.40)$$

The grid is staggered in time and space (the so-called Yee mesh) following [15], and the equations for the other field components follow this form. With a given excitation at the input either in CW or pulsed form, the excitation may be propagated through the structure by time-stepping through the entire grid repeatedly. This first-order difference formulation is second-order accurate. In the interest of time and computational speed, most of the computations in the integrated optics area are in two dimensions. Higher-order formulations are also available but the overhead that is carried slows down the marching algorithm, while improving accuracy for a specific grid size. The integrated form of the curl equations leads to a finite volume formulation. Again, a marching algorithm is developed on a split grid, as above. A recent two-dimensional alternative to the above first-order formulation, as applied

to optical guides, is the higher-order compact algorithm based on the split operator technique of Strang [16] and Shang [17]. In this approach, two fields, for example E_z and B_x , are combined to define a Riemann time invariant variable, and the propagation of this variable uses the piecewise parabolic approximation suggested by Woodward and Colella [18]. Since the algorithm is two-dimensional, the run times are smaller, and because of the parabolic approximation, higher-order accuracy is obtained without the overhead of the higher-order formulation.

2.2.3.4 Beam Propagation Method (BPM)

One of the fundamental aspects in integrated optics is the analysis and simulation of electromagnetic wave propagation in photonics devices based on waveguide geometries, including optical waveguides. The problem is to be solved such as for a given arbitrary distribution of refractive index $n(x, y, z)$, and for a given wave field distribution at the input plane at $z = 0$, $E(x, y, z = 0)$, the spatial distribution of light $E(x, y, z)$ at a generic point z must be found. In this case, the distribution of the refractive index is known, which defines the optical circuit. When a light beam is injected at $z = 0$, the problem is to determine the light intensity distribution at the exit, and in particular, what will be the output light intensity in each of the output branches.

The *Beam Propagation Method* is useful to study the light propagation in integrated photonics devices based on optical waveguides with the help of a paraxial form of the Helmholtz relation, known as the Fresnel equation. This relation is valid for paraxial propagation in slowly varying optical structures, which is the starting point to develop BPM algorithms.

The solution to the Helmholtz equation or the Fresnel equation applied to optical propagation in waveguides is known as the beam propagation method (BPM) [19]. Two numerical schemes have been used to solve the Fresnel equation. In one numerical scheme, optical propagation is modeled as a plane wave spectrum in the spatial frequency domain, and the effect of the medium inhomogeneity is interpreted as a correction of the phase in the spatial domain at each propagation step. The use of the fast Fourier techniques connects the spatial and spectral domains, and this method is therefore called Fast Fourier transform BPM (FFT-BPM). The propagation of EM waves in inhomogeneous media can also be described directly in the spatial domain by a finite difference (FD) scheme [19]. This technique allows the simulation of strong guiding structures, and also of structures that vary in the propagation direction. The beam propagation method which solves the paraxial form of the scalar wave equation in an inhomogeneous medium using the finite difference method is called finite difference BPM (FD-BPM). Also methods based on finite differences which solve the vector wave equation, called finite difference vector wave BPM (FDVBPM), have been developed. There is an intermediate approximation, which starts from the wave equation but ignores coupling terms between the transversal components of the fields, and

for that reason, this method is usually referred to as finite difference semi-vector BPM (FD-SVBPM).

The BPM is one of the commonly used numerical tools for modeling structures that are nonuniform in propagation direction for time harmonic optical signals. Since the optical carrier frequency is usually very large compared to the signal bandwidth modeling with a monochromatic wave is sufficiently accurate for many devices. Commercialized computer-aided design software (e.g., OptiWave, RSoft, and BBV) based on this technique is available and their capabilities concerning wide-angle problems, bidirectional propagation, and anisotropy are steadily improved.

In this reported work, beam propagation method has been used for mode propagation in planar waveguide sensor and using optiBPM software (version 9.0) we have prepared the layout of the proposed waveguide sensor which is discussed in Chap. 3.

2.3 Optical Sensor and Its Classification

It is important to discuss the basic characteristics of an optical sensor. The following uniquenesses of optical sensor make them advantageous over other types of sensors:

- (i) Optical sensors are highly sensitive and precise. Such sensors use an add-layer which has the ability to attract the analytes more effectively. This increases the sensitivity of a sensor to a particular analyte. Although other types of sensors such as electronic-based sensors could also employ this technique, they traditionally suffer from a major problem of electromagnetic noise [20].
- (ii) Fabricating an optical sensor is more cost-effective feasible than that of other existing optical sensors such as waveguide sensor which can be easily integrated on to a chip [21].
- (iii) Multichannel sensing can be done by optical sensors due to its compactness [22, 23]. Microfluidic channels are also one of the current developments in the industry where analytes can be flown in the fluids and due to the shift in the resonant wavelength of the analytes, sensing becomes a possibility [24].
- (iv) Another attractive application of optical sensor is its compatibility with fiber optic technology. This integration helps in the reduction of problems dealt with optical inputs and outputs by not integrating them as separate light sources [22–25].
- (v) The response time in an optical sensor is much shorter compared to that of other existing sensors [26].
- (vi) Optical sensors are highly immune to electromagnetic disturbances.

Optical sensors can be classified based on their sensing mechanisms and architectures. Fluorescence, Surface Plasmon Resonance (SPR), Raman scattering, absorption change, photon migration spectroscopy, and change in effective index are a few of the sensing mechanisms that optical sensors follow [20]. Interferometer, anti-resonant reflecting optical waveguides (ARROW), hollow waveguides, Bragg gratings, slot waveguides, ring resonator, photonic crystals, meta-materials, and low optical overlap mode (LOOM) structures are examples of the various architectures that optical waveguides employ [20–26]. There are mainly two types of optical sensor: optical fiber sensor and planar waveguide sensors.

Recently, optical waveguide sensors are preferred for different applications due to higher sensing region in its compact size in comparison with optical fiber sensors.

2.3.1 Fiber Optic (FO) Sensors and Classification

Fiber optic sensors are excellent candidates for monitoring environmental changes and they offer many advantages over conventional electronic sensors as listed below:

1. Easy incorporation into a wide variety of structures, including composite materials, with little interference due to their small size and cylindrical geometry.
2. Inability to conduct electric current.
3. Immune to electromagnetic interference (E.I) and radio frequency (R.F) interference.
4. Lightweight and high sensitivity.
5. Multifunctional sensing capabilities such as strain, pressure, corrosion, temperature, and acoustic signals.

To date, fiber optic sensors have been widely used to monitor a wide range of environmental parameters such as position, vibration, strain, temperature, humidity, viscosity, chemicals, pressure, current, electric field, and several other environmental factors [27–29].

Fiber optical sensors are divided into two basic classes referred to as intrinsic or all-fiber, and extrinsic or hybrid sensors. The intrinsic fiber optical sensor has a sensing region within the fiber and light never goes out of the fiber. In extrinsic sensors, light has to leave the fiber and reach the sensing region outside, and then comes back to the fiber [31]. Furthermore, fiber optical sensors can also be classified under three categories [30]: the sensing location, the operating principle, and application.

On the basis of sensing location, there are three types of fiber optical sensor—point sensor, distributed sensor, and quasi-distributed sensors in which both point and distributed sensing location are used for the measurement. Based on the

operating principle and demodulation technique, a fiber optic sensor can be further divided into intensity, phase, frequency, and polarization sensor. Based on the application, a fiber optic sensor can be classified as follows:

- Physical sensors: Used to measure physical properties such as temperature and stress
- Chemical sensors: Used for pH measurement, gas analysis, spectroscopic studies, etc.
- Biomedical sensors: Used in bio-medical applications such as measurement of blood flow and glucose content

2.3.1.1 Intensity-Based Fiber Optic Sensor

Intensity-based fiber optic sensors rely on signal undergoing some loss. They are made by using an apparatus to convert what is being measured into a force that bends the fiber and causes attenuation of the signal. Other ways to attenuate the signal is through absorption or scattering of a target. The intensity-based sensor requires more light and therefore usually uses multimode large core fibers [32]. The advantages of these sensors are simplicity of implementation, low cost, possibility of being multiplexed, and ability to perform as real distributed sensors. The disadvantages are relative measurements and variations in the intensity of the light source may lead to false readings, unless a referencing system is used [33, 34].

Another type of intensity-based fiber optic sensor is the evanescent wave sensor that utilizes the light energy which leaks from the core into the cladding. These sensors are widely used as chemical sensors. The sensing is accomplished by stripping the cladding from a section of the fiber and using a light source having a wavelength that can be absorbed by the chemical that is to be detected. The resulting change in light intensity is a measure of the chemical concentration. Measurements can also be performed in a similar method by replacing the cladding with a material such as an organic dye whose optical properties can be changed by the chemical under investigation [35].

2.3.1.2 Wavelength-Modulated Fiber Optic Sensors

Wavelength-modulated sensors use changes in the wavelength of light for detection. Fluorescence sensors, black body sensors, and the Bragg grating sensor are examples of wavelength-modulated sensors. Fluorescent-based fiber sensors are being widely used for medical applications, chemical sensing, and physical parameter measurements such as temperature, viscosity, and humidity.

The most widely used wavelength-based sensor is the Bragg grating sensor. Fiber Bragg gratings (FBGs) are formed by constructing periodic changes in index of refraction in the core of a single-mode optical fiber. This periodic change in index of refraction is normally created by exposing the fiber core to an intense

interference pattern of UV energy. The variation in refractive index so produced forms an interference pattern which acts as a grating.

2.3.1.3 Phase-Modulated Fiber Optics Sensors

Phase-modulated sensors use changes in the phase of light for detection. The optical phase of the light passing through the fiber is modulated by the field to be detected. This phase modulation is then detected interferometrically, by comparing the phase of the light in the signal fiber to that in a reference fiber. In an interferometer, the light is split into two beams, where one beam is exposed to the sensing environment and undergoes a phase shift, and the other is isolated from the sensing environment and is used for as a reference. Once the beams are recombined, they interfere with each other [36, 37]. Mach–Zehnder, Michelson, Fabry–Perot, Sagnac, polarimetric, and grating interferometers are the most commonly used intereferometers.

There are similarities and differences between the Michelson and Mach–Zehnder interferometers. In terms of similarities, the Michelson is often considered to be folded Mach–Zehnder, and vice versa. Michelson configuration requires only one optical fiber coupler. Because the light passes through both the sensing and the reference fibers twice, the optical phase shift per unit length of fiber is doubled. Thus, the Michelson can intrinsically have better sensitivity. Another clear advantage of the Michelson is that the sensor can be interrogated with only a single fiber between the source-detector module and the sensor. However, a good-quality reflection mirror is required for the Michelson interferometer [27].

2.3.1.4 Polarization-Modulated Fiber Optic Sensors

The direction of the polarization of the electric filed of the light field is defined as the polarization state of the light field. There are different polarization states of the light field—linear, elliptical, and circular polarization states. For the linear polarization state, the direction of the electric field always keeps in the same line during the light propagation.

For the elliptical polarization state, the direction of the electric field changes during the light propagation. The end of the electric field vector forms an elliptical shape; hence, it is called ‘elliptical polarized light.’ The refractive index of a fiber changes when it undergoes stress or strain. Thus, there is an induced phase difference between different polarization directions. This phenomenon is called photoelastic effect. Moreover, the refractive index of a fiber undergoing a certain stress or strain is called induced refractive index. The induced refractive index changes with the direction of applied stress or strain. Thus, there is an induced phase difference between different polarization directions. In other words, under the external perturbation, such as stress or strain, the optical fiber works like a linear retarder. Therefore, by detecting the change in the output polarization state, the external perturbation can be sensed [27].

2.3.2 *Integrated Optic Waveguide Sensors*

The basic principles of planar waveguide sensors are same as that for the fiber optic sensors. The two fields have been developed at different paces and with slight different targets. Fibers have the unique capability of operating overextended gauge lengths (even km!) in either point sensing or distributed sensing format. In the former case, the FOS is configured in such a way that monitoring of the measurand occurs at a specified location along the fiber; in the latter case, light is guided by confining it in optical structures known as waveguides by utilizing the total internal reflection principle.

Light is confined within the waveguide along the dimensions of 1D, 2D, or 3D. So planar waveguide can be classified based on the dimensions of the light that is confined as planar waveguides (1D), channel waveguides (2D), and photonic crystals (3D), respectively.

Channel waveguides known as 2D waveguides are those which have a higher refractive index in the core when compared to substrate and cover. In this type of structure, the Total Internal Reflection (TIR) takes place at the interfaces and also at the lateral boundaries. The refractive index of the core region is always maintained more than the refractive indices of surrounding regions. The channel waveguides can be classified into a similar manner to planar waveguides in terms of step index or graded index or symmetric/asymmetric except that we have to consider the addition of one extra dimension. Three main types of channel waveguides have been in use, namely stripe waveguide, ridge waveguide, and buried waveguide, respectively.

Integrated Optic (IO) planar waveguides can be fabricated with a variety of materials such as SiON/SiO_2 , $\text{GeO}_2\text{--SiO}_2/\text{SiO}_2$, GaAsInP/InP , Ti: LiNbO_3 , SOI, and polymers. Its greater advantage is that it permits flexibility both in design and in manufacturing by exploiting the combination of thin film technology with other planar waveguide technologies, such as surface acousto-optic interaction, laser writing, silicon micromachining, micro-electromechanical systems (MEMS), and optoelectronic integration on a semiconductor substrate. Since IOSs as a temperature and a displacement sensor were first reported in 1982 [38, 39], afterward many other integrated optical devices for sensing application have been proposed and demonstrated [40–42]. The detail of integrated optic planar waveguide sensor is discussed in the subsequent Sect. 2.3.2.1. In the following sections, some examples of IOSs are very briefly presented and discussed.

2.3.2.1 *Integrated Optical Interferometers*

Mach-Zehnder Interferometers (MZI) based on integrated optics are easily fabricated, by means of standard integrated circuit (IC) technologies and are one of the most common structures exploited for the detection of the phase shift induced by a

measurand. Several sensing devices have been demonstrated, e.g., for the detection of displacement, for refractometry, and for biosensing [43, 44].

2.3.2.2 Grating-Coupler Sensors

In integrated optics, the light is launched into the thin-film waveguide by prism coupling, grating coupling, or fiber-to-waveguide butt coupling [45]. The prism coupling is the most common technique in the laboratory, whereas grating couplers can be fabricated directly on top or inside the waveguide itself, offers a more robust mechanism for practical application. Grating coupling, however, is not simply another way of performing the access function to/from an optical waveguide. As their operation depends critically on the refractive indices of the guiding film and that of surrounding media (once the wavelength is fixed), the precise measurement of the in-coupling angle constitutes a sensitive tool to detect changes in refractive index or wavelength induced by a measurand [46]. Commercial grating coupler sensor chips are available. The cladding layer modifies the optical, chemical, or biochemical properties of the surface of the chip. A wide choice of coatings, from thin films of SiO_2 , TiO_2 , TaO_2 , ITO (Indium Tin Oxide), ZrO_2 to thick films of PTFE, silicone, etc., are used. The biosensing application of grating coupler sensors includes adsorption of protein at surface, immunosensing, drug screening, analysis of association and dissociation kinetics, and many more. Typical size of the chip is 48 mm (length) \times 16 mm (width) \times 0.55 mm (thickness), and the guiding sol-gel layer has thickness in the range 170–220 nm; grating area is 2 mm (L) \times 16 mm (W), its depth (the grating is a surface relief structure) is about 20 nm, and its pitch is $\approx 0.4 \mu\text{m}$.

2.3.2.3 Evanescent Wave and Surface Plasmon Resonance Sensors

The origin of the evanescent wave may be explained as follows: When light propagates in an optical fiber or waveguide, a fraction of the radiation extends a short distance from the guiding region into the medium of lower refractive index which surrounds it. This evanescent wave which decays exponentially with distance from the waveguide interface defines a short sensing volume within which the evanescent energy may interact with molecular species. Recently, optical waveguide sensors based on such evanescent wave (EW) interactions have attracted significant research interest [47, 48].

The impetus behind adopting the EW approach derives from a number of advantages offered by the technique in particular applications:

- (i) Because the interrogating light remains guided, no coupling optics is required in the sensing region and an all-fiber approach is feasible. Furthermore, considerable miniaturization is possible for which EW interactions are predominant sensing mechanisms.

- (ii) The technique can provide enhanced sensitivity over conventional bulk optics approaches.
- (iii) In contrast to other sensing methods, EW approach affords the sensor designer greater control over interaction parameters such as interaction length, sensing volume, and response time.

The control over the degree of penetration of the EW into the low index medium is characterized by the penetration depth d_p , which is the perpendicular distance from the interface at which the electric field amplitude, E , has fallen to $1/e$ of its value, E_0 , at the interface, i.e.,

$$E = E_0 \exp(-z/d_p) \quad (2.41)$$

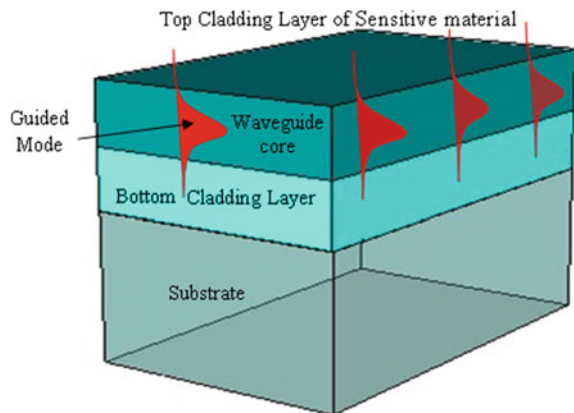
The magnitude of the penetration depth is given by:

$$d_p = \frac{\lambda}{2\pi n_1 \left[\sin^2 \theta - \left(\frac{n_2}{n_1} \right)^2 \right]^{1/2}} \quad (2.42)$$

where λ is the vacuum length, θ is the angle of incidence to the normal at the interface, and n_1, n_2 are the refractive index values of the dense and rare media, respectively. Although d_p is less than λ , it is clear from Eq. (2.42) that its value rises sharply as the angle of incidence approaches the critical angle, $\theta_c = \sin^{-1} \left(\frac{n_2}{n_1} \right)$. This Eq. (2.42) highlights the importance of the interface angle θ in the design of EW sensors.

Figure 2.11 depicts a typical sensor which employs the evanescent sensing technique. When the total internal reflection take place at an angle larger than the critical angle, the evanescent field decays exponentially. In the structure, Silicon is used as the substrate material. A sensitive material is used on top of the waveguide

Fig. 2.11 Evanescent wave sensor



material called as an adlayer to help attract analytes easily and effectively. This increases the sensitivity.

Figure 2.12a depicts the angle of the incident light being less than the critical angle. Figure 2.12b depicts the incident angle equals the critical angle. For total internal reflection, the angle of the incident ray must be greater than the critical angle, which is depicted by Fig. 2.12c.

Thus, the evanescent wave is formed and it penetrates into the region of lower refractive index. The species to be detected are made to interact with the evanescent field that penetrates into the cladding region. Strong evanescent wave absorption occurs when the peak absorbance wavelength of the analytes equals the wavelength of the light that is propagated [49–52]. Further criteria about the material selection are discussed later in this chapter.

Figure 2.13 shows the phenomenon of evanescent wave sensing along with the determination of the penetration depth. A ray of light is incident upon the reflecting plane with an angle θ_i , whereas n_2 is the refractive index of the cladding which is air. n_1 is the refractive index of the core region. According to the principle of total internal reflection, n_1 is greater than n_2 . This penetration depth can be measured using Eq. (2.43) if we have the knowledge of operating wavelength and refractive indices of core and cladding regions.

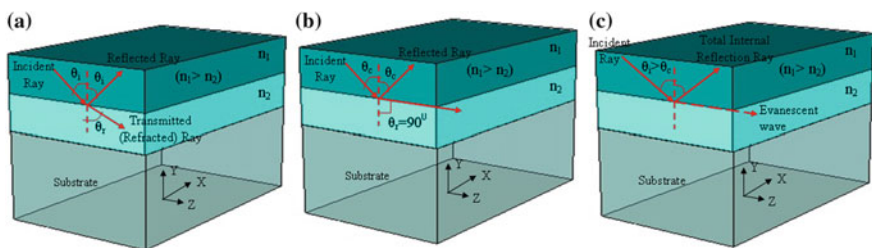
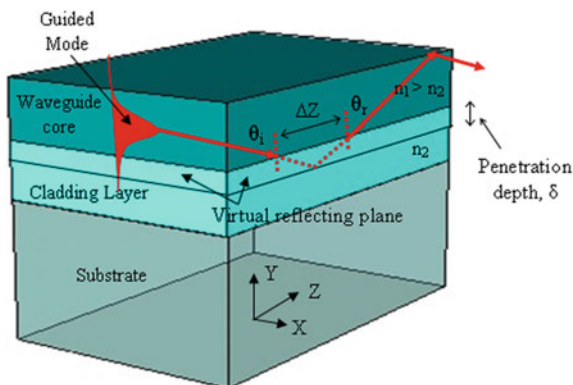


Fig. 2.12 Formation of evanescent wave

Fig. 2.13 Penetration depth



The penetration depth of electric field in the region can also be determined as [53, 54],

$$\delta = \left(\frac{\lambda}{2\pi} \right) [N^2 - n_c^2]^{-1/2} \quad (2.43)$$

where δ is the penetration depth which determines the exponential decay of the electric field

λ wavelength of operation

N effective refractive index of the core, and

n_c refractive index of the cladding region

In Fig. 2.11, it is shown that in the sensing region, the measurand acts as cladding region, and hence, the evanescent lightwave propagation depends on measurand that interacts with evanescent waves. The change in a chemical or physical parameter of the cladding or sensing region is converted into an optically measurable quantity by means of a change in absorption of the guided wave or in its effective index [47]. Such sensing structure relies on measurand-induced changes of the field profile of the guided mode; this is in contrast to the refractive IO sensors in which the changes of the effective refractive index n_{eff} are exploited [55].

The technique which is becoming a key tool for characterizing biomolecular interaction is that based on Surface Plasmon Resonance (SPR) [56]. The optical excitation of surface Plasmon by the method of Attenuated Total Reflection (ATR) was demonstrated in the late Sixties, and very soon it was applied for characterization of metal thin films [57]. In early Eighties, the use of SPR for gas sensing and biosensing was demonstrated [58–60] and since then SPR sensor technology has continued to grow up [61] and it is now commercialized.

2.3.3 Basic Principle: Optical Planar Waveguide Sensors

Although trapped within the dielectric medium of the optical waveguide, the radiation that propagates inside the waveguide can be perturbed by the external environment, and this perturbation can be used to draw useful information for sensing purposes. In fact, the interaction of the parameter of interest that is the measurand with the waveguide produces a modulation in the propagation constants of the guided light beam. That modulation represents the sensitive function of the measurand of interest.

The basic elements constituting a guided wave sensor are an optical source, an optical interface for source-to-waveguide light coupling, the waveguide itself where the measurand-induced light modulation occurs, a photodetector and the electronics for amplification, signal processing, and data display. In accordance with the optical parameter, which is modulated by the measurand, waveguide sensors can be divided into four basic categories:

- Phase-modulated,
- Polarization-modulated,
- Wavelength-modulated, and
- Intensity-modulated.

Waveguide sensors are further subdivided as intrinsic, extrinsic, or evanescent wave sensors. Intrinsic sensors are true waveguide sensors in which the sensing element is the waveguide itself. Extrinsic sensors make use of an optical transducer coupled with waveguide, the optical constants of which are modulated by the measurand. Evanescent wave sensors are hybrid intrinsic/extrinsic sensors, since measurand-induced modulation occurs in the waveguide itself, in most cases because of the presence of a measurand-sensitive cladding section.

2.3.3.1 Integrated Optic Planar Waveguide Sensor Effect

The integrated optic planar waveguide sensors make use of guided waves or modes in optical waveguides; in particular of the orthogonally polarized TE_0 and TM_0 modes of high refractive index. The modes in planar optical waveguides are TE_m (transverse electric or s-polarized) and TM_m (transverse magnetic or p-polarized), where $m = 0, 1 \dots$ is the mode number. It is seen in sensor applications that the effective refractive index N is the most main physical quantity of the guided modes. The modes propagate down the waveguide with the phase velocity, $v_p = c/N$, where c is the velocity of light in vacuum and N is the effective refractive index of the mode; N depends on polarization (TE or TM), mode number m , wavelength λ , the properties of the wave guiding film F, and on the refractive indices n_s and n_c , respectively, of the substrate S and of the medium C covering the waveguide. The field of a guided wave penetrates as an evanescent wave, traverses a small distance into the medium which in sensor applications is the sample covering the waveguide. More precisely, the evanescent field decays exponentially proportional to $\exp(-z/\Delta z_c)$ (say) with distance z from the waveguide surface, where

$$\Delta z_c \equiv (\lambda/2\pi) [N^2 - n_c^2]^{1/2} \quad (2.44)$$

is the penetration depth. The basic IO sensor effect is caused by interaction of the evanescent wave of the guided mode with the sample [54]. The evanescent field ‘senses’ the changes in the refractive index distribution near the waveguide surface. Thus, changes in the effective refractive indices of the guided modes are induced. This is the primary IO sensor effect.

The effective refractive index changes (N) can be induced by two different effects as follows:

- (i) the formation of an adlayer, transported from the bulk of the sample to the waveguide surface.
- (ii) changes Δn_c of the refractive index n_c of the homogeneous (liquid) sample C covering the waveguide surface.
- (iii) the adsorption or desorption of molecules in pores of the wave guiding film F and leads to an effective refractive index change ΔN .

When all the effects (i)–(iii) are present, the resulting effective refractive index changes are as follows:

$$\Delta N = \left(\frac{\partial N}{\partial d_F} \right) d_F + \left(\frac{\partial N}{\partial n_c} \right) \Delta n_c + \left(\frac{\partial N}{\partial n_F} \right) \Delta n_F \quad (2.45)$$

In the above Eq. (2.45), sensitivity constants $\left(\frac{\partial N}{\partial d_F} \right)$, $\left(\frac{\partial N}{\partial n_c} \right)$, and $\left(\frac{\partial N}{\partial n_F} \right)$ are the differential changes in effective refractive index of a guided mode for a small change in:

- (i) the thickness d_F of an adsorbed or bound adlayer F’;
- (ii) the refractive index n_c of the (liquid) sample;
- (iii) the refractive index n_F of the microporous waveguide film F.

The optical sensitivity constants have been calculated using two independent methods [62–64]. In the history of the basic IO sensor effect, the dependence of the optical sensitivity constants on waveguide parameters has some bearing discovered, by serendipity. Originally, the object of this work [65, 66] was actually to find out whether or not grating couplers could be fabricated on dip-coated SiO_2 – TiO_2 waveguides. The first IO sensor experiment was reported at the European Conference on Integrated Optics held in Florence in 1983 [67]. Nowadays, this experiment is routinely performed to demonstrate the basic IO sensor effect [68–70].

2.3.3.2 Requirement of IO Planar Waveguide Sensors

For the purpose of improving performance and throughput, to a great extent reported work at present has focused on miniaturization of sensors. The benefits of miniaturization, such as minimal sample requirements, reduced reagent consumption, decreased analysis time; higher levels of throughput and automation can be effortlessly achieved with integrated optic sensing technology. In clinical diagnostics and in adulteration detection these days, there is need for extreme sensitivities. Because IO sensors are small, they also proffer the possibility to realize multipurpose sensor arrays and the way is open for a cheap mass production similar to the way electronic chips are produced nowadays. It is not indispensable for the sensor industry to put up with all the cost of the research and development of IO devices and systems by itself. As a result, we can conclude that there are ample reasons why IO sensors should have our attention: An IO sensor, to our estimation, is likely to take part in a very significant role in the future.

2.3.4 Comparison Between Fiber Optic Sensor and Integrated Optical Planar Waveguide Sensor

Even after a number of years of development, at a standstill fiber optic sensors have not enjoyed grand commercial success, since it is not simple to put back already well-established technologies, even if they reveal certain limitations. Fiber optic sensors have attracted considerable attention, especially in the application of biochemical species detection having exceptional advantages such as good compactness and high sensitivity, shorter response time, low cost, and high compatibility with fiber optic networks. However, optical fiber-based systems do not seem promising with respect to fabrication, efficiency, and miniaturization. However, planar waveguide-based platforms employing evanescent wave sensing techniques have shown tremendous improvement [71] and evanescent wave sensors have proven to be highly sensitive [72–74].

2.4 Performance Parameters of Optical Sensors

Optical sensor performance is determined by a number of parameters [75, 76] such as sensitivity, limit of detection (LOD), limit of quantization (LOQ), and specificity/selectivity that are summarized as follows:

2.4.1 Sensor Sensitivity

Sensitivity is the change of the sensor output signal in response to a change in a property of the sensor (e.g., the concentration of an analyte deposited on the sensor surface). It is a parameter that defines the ability of a sensor to transduce an input signal (which is the variation of a sensor property) to an output one. Different definitions of sensitivity such as waveguide sensitivity, etc., can be found in the literature in relation to the parameter representing the changing property, i.e., the input signal. If the sensor interacts with an analyte in contact with its surface, the mass/sensor surface unit ratio can be assumed as input variable. In case of sensors sensitive to an analyte bound to the surface, the input signal is the concentration of the analyte. In this case, the parameter takes also into account some aspects such as the total exposed area and the kinetics of the binding between the sensor and the analyte.

2.4.2 Limit of Detection (LOD)

Limit of detection (LOD) is defined as the minimum amount of concentration or mass of the biochemical substance that can be detected by the sensor over the background signal. Limit of detection depends on the resolution of the sensor. Resolution is the smallest change that can be observed in the output signal. It is a critical performance parameter for detecting analytes at low concentration or molecules at low weight and depends on transducer, read-out technique, overall noise level, and data processing.

2.4.3 Limit of Quantization (LOQ)

An additive figure used to describe the smallest concentration of a measurand that can be measured by an analytical procedure is the limit of quantization (LOQ). It is defined as the lowest concentration at which not only the analyte can be reliably detected, but also at which some predefined goals concerning measurement errors, i.e., bias and imprecision, are met. The dynamic range is the range of the measured values detectable by the sensor. It is lower limited by the LOD and upper limited by the saturation of the sensing signal sensor or by the physical limitation such as sensor breakage or unpredictable changes of the sensitivity.

2.4.4 Selectivity or Specificity

In addition to being able of producing an output signal related to the presence of an analyte, a sensor must also be able to distinguish between the analyte and any other substance. This capability is named selectivity or specificity, which is difficult to be measured due to the very large number of possible substances that do not generate an output signal. In fact, the sensor selectivity becomes particularly important when trying to detect an analyte at low concentration in an environment containing a high concentration of other materials, many of which cannot specifically bind to the sensor and therefore can produce an anomalous signal. Many biosensors exploit complex, specific binding interactions provided by nature, such as antibody–antigen, nucleic acid hybridization, biotin–streptavidin, and enzyme–substrate interactions. Other substances such as aptamers have been artificially developed for the same purpose.

2.4.5 Sample Volume

The sample volume is the least-requested volume to make a consistent measurement. Other aspects, such as portability and cost, can have a major impact on the commercial success of a sensing technique. Portability refers to the possibility to easily carry the biosensors. It is important for real-time detection when time and location are critical aspects, such as in the case of difficult transportation of the sample to the laboratory. Cost is determined by the disposable and by the instrumentation. Although the optical technologies are in principle more advantageous in terms of cost for performing an individual assay because they do not use tag reagents, the cost of the transducer has to be low enough. This can be achieved, as an example, by designing a sensor, even using an expensive technology that can be regenerated and used for several successive analyses.

2.5 Review on Planar Waveguide Materials and Fabrication Technologies

This book explores the interesting possibility to fabricate state-of-the-art SiON-based planar waveguide sensor with potentially low cost and by applying the standardized processes using SiO₂/SiON as a waveguide material.

Table 2.1 illustrates the optical properties and fabrication steps of different waveguide materials used for fabrication of PID's [77]. It is found from the table that the fabrication steps of waveguide devices used for silicon-based materials are as same as those used for conventional IC technology but those are not the same for other waveguide materials as mentioned in Table 2.2. The fabrication steps of silicon-based materials can easily be adapted in mass production which is commercially viable. Since InP/GaAsInP waveguide materials use molecular beam epitaxial (MBE) growth technique, the fabrication cost of InP/GaAsInP waveguide is more than other materials. The basic fabrication step for polymeric waveguide materials is LASER writing which is cheaper; therefore, it is difficult to use the same technology for mass production. Moreover, LASER writing technique is time consuming.

Table 2.1 also demonstrates that high-index contrast is available in SiO₂/SiON, InP/GaAsInP, SOI, and polymeric waveguide materials to compact waveguide device components, compared to Ti:LiNbO₃ and SiO₂/SiO₂-GeO₂ materials having lower index contrast. In addition, these materials show polarization insensitive property in comparison with Ti:LiNbO₃ material because of crystal structure. Actually, polymeric and silicon-based materials show thermo-optic properties. Although polymeric materials have higher thermo-optic coefficient and easy processing of devices, silicon-based materials are highly stable and compatible to conventional IC processing technology.

Table 2.1 Waveguide materials and its properties and fabrication steps

Materials with range of refractive index	Δn (max)	Δn taken by previous authors	Properties				Basic steps of fabrication	Material cost/ processing cost	Reported sensing application
			Thermo-optic coefficient $\alpha = \frac{dn}{dT}$	Electro-optic coefficient (r_{33})	Stability	Polarization sensitivity/birefringence			
SiO ₂ /SiON index range ~ (1.45–1.98)	~0.53	0.033 [79] 0.103 [80]	10 ⁻⁵ /°C [81]	–	High [81]	Polarization insensitive [81]/10 ⁻⁶	(i) Formation of SiO ₂ lower cladding layer on Si-substrate (ii) Formation of SiON layer on SiO ₂ layer (iii) Fabrication of SiON core with photolithography (iv) Formation of top cladding SiO ₂ layer	Moderate/ high	–
GeO ₂ -SiO ₂ /SiO ₂ index range ~ (1.45–1.47)	~0.02	0.0075 [82] 0.0025 [83]	10 ⁻⁵ /°C [81]	–	High [81]	Polarization insensitive [81]/10 ⁻⁵	(i) Formation of SiO ₂ lower cladding layer on Si-substrate (ii) Formation of SiO ₂ -GeO ₂ layer on SiO ₂ layer (iii) Fabrication of SiO ₂ -GeO ₂ core with photolithography and RIE (iv) Formation of top cladding SiO ₂ layer	Moderate/ high	–
Silicon on insulator (SOI) (3.4767)	2.026	–	1.84 × 10 ⁻⁴ /°C [81]	–	High [81]	Polarization insensitive /10 ⁻⁴	(i) Formation of SOI wafer by using bond and etch back method or Separated by implanted oxygen method (ii) Fabrication of Si core with photolithography and RIE (iii) Formation of top cladding SiO ₂ layer	Moderate/ high	–

(continued)

Table 2.1 (continued)

Materials with range of refractive index	Δn (max)	Δn taken by previous authors	Properties				Basic steps of fabrication	Material cost/processing cost	Reported sensing application
			Thermo-optic coefficient $\alpha = \frac{dn}{dT}$	Electro-optic coefficient (r_{33})	Stability	Polarization sensitivity/birefringence			
Ti: LiNbO ₃ index range ~ (2.15–2.21)	~0.06	0.006 [84] 0.01 [85]	–	30.8 pm/V [8]	High [8]	Polarization sensitive [8]/10 ⁻²	(i) Formation of Ti: LiNbO ₃ using thermal Ti diffusion (ii) Fabrication of waveguide core with photolithography and etching	High/high	–
InP/GaAsInP index range ~ (3.13–3.5)	~0.33	0.13 [86] 0.167 [87] 0.15 [88] [89]	–	–	Stable [86]	Polarization insensitive [86] /2.5 × 10 ⁻⁴	(i) Formation of GaAsInP layer by using molecular beam epitaxial growth (MBE) (ii) Formation of InP layer by using MBE (iii) Fabrication of waveguide core with photolithography and etching	High/high	–
Polymer index range ~ (1.44–1.65)	~0.21	0.03–0.1 [90]	10 ⁻⁴ /°C [90]	10–200 pm/V	Low	Polarization insensitive /10 ⁻² –10 ⁻⁶	(i) Fabrication of polymer layers by using chemical processing polymerization (ii) Fabrication of polymeric waveguide by using LASER writing	Low/low	–

Table 2.2 Characteristics of optical sensors as reported by different authors

Author's name/material used	Type of waveguide structure	Core size and cladding width (μm) ²	Sensitivity	Wavelength of light source	Application	Fabrication cost
Kumar et al. [91] Glass/Silver	Planar waveguide	0.5×0.03 (μm) ²	5.36×10^{-4} nm	0.6328 μm	–	High
Parriaux et al. [92]	Planar waveguide	–	–	–	–	Moderate
Taya et al. [93] Si ₃ N ₄	Planar waveguide	–	–	–	–	High
Carlos et al. [94] Si ₃ N ₄ /SiO ₂	Slot waveguide	–	1.8 and 3.2 nm/ (ng/mm ²)	1.3 μm	Detection of bovine serum albumin and anti-BSA, respectively	Moderate
Karaskinski [95] SiO ₂ :TiO ₂	Planar waveguide	–	0.113 and 0.147	677 nm	Chemical and biochemical measurements	Moderate
Carlos [96] SiO ₂ /Si ₃ N ₄ and Si/SiO ₂	Slot waveguide	–	212 nm/RIU	1.55 μm	Biochemical sensing	Moderate
Densmore et al. [97] SOI	Planar waveguide	–	0.31	1550 nm	Biochip applications	High
Karaskinski [98] SiO ₂ :TiO ₂	Planar waveguide	–	3×10^{-3} (TM1) 1.4×10^{-3} (TE1)	677 nm	Chemical and biochemical measurements of water solutions	High
Sofyan and Taher [99] water/ZeSe/ideal plasma	Planar waveguide	–	–	1550 nm	Characterization of plasma media	High
Renling et al. [100] B270 optical glass/composite salt 0.004 AgNO ₃ -0.996 NaNO	Planar waveguide	–	–	632.8 nm	–	High

(continued)

Table 2.2 (continued)

Author's name/material used	Type of waveguide structure	Core size and cladding width (μm)	Sensitivity	Wavelength of light source	Application	Fabrication cost
Yimit et al. [101] potassium-ion-exchanged (K+) glass	Planar waveguide	–	10 ^{−4}	633 nm	(bio-)chemical sensing	High
Airoudj et al. [102] polyaniline (PANI)/polymethyl methacrylate (PMMA)	Planar waveguide	–	17 % for LI = 5 mm and 6 % for LI = 2 mm	632.8 and 980 nm	Ammonia detection	Moderate
Veldhuis et al. [103] InP/GaAsInP	Planar waveguide	–	1.35	1550 nm		High

Although SOI has higher index contrast of fixed value ~ 2 , wide variation of the index contrast (maximum up to 0.53) can be achieved by varying nitrogen and oxygen contents in SiON material. In the case of SOI waveguide device, the reported propagation loss of SOI waveguides is 0.1 dB/cm [78] and the fiber-to-chip coupling loss is of the order of 2–5 dB/facet, whereas in the case of SiO₂/SiON, the propagation losses are same as SOI materials but fiber-to-chip coupling loss (order of 1 dB per facet) is lower than that of SOI material. The SiO₂/SiON material also shows more chemical inertness property than SOI material. Moreover, the processing system of SiO₂/SiON waveguide device is available with us for fabrication of waveguide devices. Because of the above reasons, we have chosen SiO₂/SiON as waveguide material in which SiON material is used for core fabrication of the planar waveguide as mentioned in detail in Chap. 4, respectively.

2.6 Optical Planar Waveguide Sensor and Applications—A Review Study

Table 2.3 shows different optical planar waveguide sensors reported by previous author. Very few studies have been reported for integrated planar waveguide optical sensor. Kumar and Singh [91] reported the analysis of the sensitivity of a five-layer metal-clad planar waveguide-based sensor having nonlinear material in the cover media. It has been shown that the introduction of the nonlinear material in the waveguide not only improves the sensitivity but also provides additional parameters to increase the sensitivity. Parriaux et al. [92] presented an extensive theoretical analysis for the design of evanescent linear waveguide sensors and derived the conditions for the maximum achievable sensitivity for both TE and TM polarizations. Taya et al. [93] has shown that the sensitivity of an optical waveguide sensor can be dramatically enhanced by using a meta-material with negative permittivity and permeability. Carlos et al. [94] has demonstrated label-free molecule detection by using an integrated biosensor based on a Si₃N₄/SiO₂ slot waveguide microring resonator. Karasinski [95] presented planar waveguide sensor structures with grating couplers for the application in evanescent field spectroscopy. Planar slab waveguides of high refractive index ($n \approx 1.8$) were produced in sol–gel technology. The layers SiO₂:TiO₂ were coated on BK7 glass substrate using dip-coating method. Since the structure is fabricated by sol–gel technology but not by conventional IC technology, it can not have mass production. Carlos [96] has shown that the use of slot waveguides has proven to be advantageous over conventional waveguides in terms of sensitivity and potential use in applications requiring the fusion of nano-photonics and nano-fluidics. Densmore et al. [97] demonstrated a

Table 2.3 Different adulteration detection technique as reported by previous authors

Author's name/material or instrument used	Type of sensor	Length of the sensor	Core size (µm) and cladding width (µm)	Numerical aperture (NA)/ microscope objective	Sensitivity	Wave length of light source	Application	Room temperature	Noticeable advantage
Kishor et al. [122]/ optical time domain reflectometer	Optical fiber-based	–	–	–	–	Pulsed laser diode at 1550 nm	Determination of adulteration in petrol	25 °C	–
Roy [119]/ plastic-clad-silica (PCS)	Fiber optic sensor		600 (µm)	0.4/20x	–	He-Ne laser at 632.8 nm	Determining adulteration of petrol and diesel by kerosene	30 °C	–
Bahari et al. [123]/ spectro-photometer	–	–	–	–	–	Spectrophotometer set at 600 nm	Determination of the adulteration of petrol with kerosene	–	Reduction of titration volume difference in batch variations
Mishra et al. [124]/ single-mode fiber (SMF-28, Corning) with a UV written long period fiber grating (LPFG)	Fiber optic sensor	–	–	–	0.12 nm		Hydrocarbon contamination study	–	Detect presence of 10 % contaminant in petrol and diesel
Patil et al. [125]/ microcontroller	Fiber optic sensor	–	488 µm × 612 µm	0.47	–	–	Adulteration detection applications	–	–

new highly sensitive evanescent field sensor using silicon-on-insulator (SOI) photonic wire waveguides. Karasinski [98] presented the results of theoretical analysis and the results of experimental research of composite sol-gel SiO_2 : TiO_2 film/ion-exchange glass optical waveguides. The theoretical part of the work presented modal characteristics and the influence of the parameters of the uniform waveguide film on homogeneous sensitivity. The fabrication cost is high. Very recently, Taya and El-Agez [99] presented an extensive theoretical treatment of an optical waveguide sensor consisting of thin dielectric film surrounded by an aqueous cladding and an ideal nonabsorbing plasma substrate. They have considered the case when the frequency of the guided light is greater than the plasma frequency so that the refractive index of the substrate is less than unity. Zou et al. [100] presented planar waveguides with Fermi-graded refractive index variation were examined as sensors for the measurement of solution concentrations. The waveguides were fabricated on B270 optical glass by an ion exchange method using the composite salt 0.004AgNO_3 – 0.996NaNO_3 . This type of sensor requires very good alignment system which can be made portable. Yimit et al. [101] presented the design and fabrication of highly sensitive thin-film composite optical waveguides (OWG) sensor device with high refractive index for sensor applications. Airoudj et al. [102] presented a new Multilayer Integrated Optical sensor (MIO) for ammonia detection at room temperature. The sensor is based on the interaction of the evanescent wave of the guided mode (orthogonally polarized TE_0 and TM_0 modes) with the sensitive material. Then, the penetration depth of the evanescent field must be higher than the passive layer thickness. Since sensing area is less, sensitivity is less than the other sensors. Veldhuis et al. [103] have shown that the sensitivity of the effective refractive index on the cladding index in evanescent optical waveguide sensors can be larger than unity. It has been shown that in the case of homogeneous sensing with a three-layer slab waveguide the sensitivity of the effective refractive index to variations of the cladding index can be larger than unity for TM polarization and strong guidance.

It is apparent from the above studies that very good planar waveguide sensor necessitates the following characteristics:

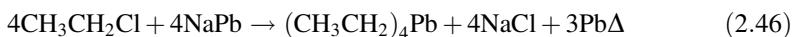
- (i) Simple structure having fewer layers for plummeting cost of fabrication.
- (ii) More sensing area for enhancement of sensitivity.
- (iii) Make use of low-cost material for reduction of fabrication cost.
- (iv) High selectivity
- (v) Use of conventional IC processing technology for mass production
- (vi) Simple alignment setup for making it portable

From the reported sensors as mentioned in Table 2.2, it is shown that no planar waveguide sensors show all the above characteristics together. So it is required to propose and develop simple planar waveguide-based sensor structure having bigger sensing area and less number of layers using low-cost materials. The use of conventional IC technology can provide its production for reduction of fabrication cost. In this book, we have tried to propose and develop the same sensors as reported in Chaps. 4, 5, and 6, respectively.

2.6.1 *Refractometric Optical Sensing and Petroleum Fuel Adulteration*

Since the proposed work consists of sensing of adulteration of petroleum products, we have tried to report previous studies on adulteration of petroleum products.

The Motor Spirit and High-Speed Diesel (Regulation of Supply and Distribution and Prevention of Malpractices) Order, 1998, defines adulteration as the introduction of a foreign substance into motor spirit/high-speed diesel, illegally or unauthorized with the result that the product does not conform to the requirements and specifications of the product. The foreign substances are called adulterants, which when introduced alter and degrade the quality of the base transport fuels. Adulteration is financially unattractive when less than 10 % while more than 30 % [104] without doubt is likely to be detected by the user from the degradation of the performance of the engine caused by the adulterated fuel. In addition, we see that the oil companies add antiknock compounds such as Tetra Ethyl Lead (TEL), $(\text{CH}_3\text{CH}_2)_4\text{Pb}$ to raise the antiknocking property.



To check the adulteration effectively, it is necessary to monitor the fuel quality at the distribution point itself. The equipment for this purpose should be portable and the measurement method should be quick, capable of providing test result within a very short time. The measuring equipment should also be preferably inexpensive (as a large number of such units would need be simultaneously deployed) and easy to use. It is found that the earlier techniques available for detecting adulteration [105–111] require taking out the sample for measurement and thus, they are time-consuming and are unable to sense adulteration level below 20 % [112]. So in our work, we try to detect adulteration of petroleum products (specially petrol with diesel, diesel with kerosene, and petrol with both kerosene and diesel) below 20 % level with accuracy, enhanced sensitivity, and minimal sample volume by using optical waveguide sensor (mentioned in Chap. 4). This technique is immunity to electromagnetic interferences, avoiding chemical hazardous. Besides all these above advantages, planar waveguide-based optical sensors offer an important key feature that the sensor is very sensitive to variation in refractive index of sensing

material surrounding the core (as cladding). Before the detection of adulteration, we like to mention chemical composition of petroleum.

Petroleum is a mixture of hydrogen and carbon starting number of carbon atoms from C_1 to C_{70} and more. The ultimate analysis of petroleum indicates that in addition to hydrocarbons (83–87 % of Carbon (C) and 11–15 % of Hydrogen (H)) small quantities of nitrogen (N), sulfur (S), and oxygen (O) are also present. Sulfur is presented generally as alkylsulfides, hydrosulfides and hydrogen sulfide, and thiophene and less frequently, combined oxygen is presented as carboxylic acids (naphthalenic acids) ($COOH$ group), ketones ($C=O$), and phenols (C_6H_5OH). The disagreeable odor of petroleum is due to the sulfur compounds present in it. The hydrocarbon present in the crude petroleum may be divided into two main classes.

Open chain or aliphatic compounds comprising

- n-paraffins series (C_nH_{2n-2}),
- isoparaffin series (C_nH_{2n+2}) and,
- olefin series (C_nH_{2n}).

Ring compounds comprising

- naphthalene series (C_nH_{2n}) (derivative of cyclopentane and cyclohexane)
- aromatic series or benzene series.

In petroleum gaseous paraffins (hydrocarbons), methane (CH_4) to butane (C_4H_{10}) is present in the dissolved state. The naphthenic hydrocarbons present in petroleum are mainly the derivatives of cyclopentane and cyclohexane. As Fig. 2.14 indicates, aromatic compounds have higher carbon-to-hydrogen (C/H) ratios than naphthenes, which in turn have higher C/H ratios than paraffins. The heavier (more dense) the crude oil, the higher its C/H ratio will be. Due to the chemistry of oil refining, the higher the C/H ratio of a crude oil, the more intense and costly the refinery processing required to produce given volumes of petrol/gasoline and distillate fuels. The proportions of the various hydrocarbon classes, their carbon number distribution, and the concentration of hetero-elements in a given crude oil determine the yields and qualities of the refined products. The petroleum fraction for petrol, kerosene, and diesel is shown in Table 2.4.

Figure 2.15 shows the stepwise process of fractional distillation for obtaining the petroleum products such as petrol, kerosene, and diesel.

2.6.1.1 Causes of Petroleum Adulteration

Most developing country governments have not yet established a system of fines that can act as a strong deterrent to fuel adulteration. There are number of reasons for this, including poor governance, shortage, or the absence of technical staff and paraphernalia for designing and conducting monitoring. Given these limitations, identifying and dealing with this abuse will require addressing problems on multiple fronts. The primary factors that encourage the practice of adulteration are the following:

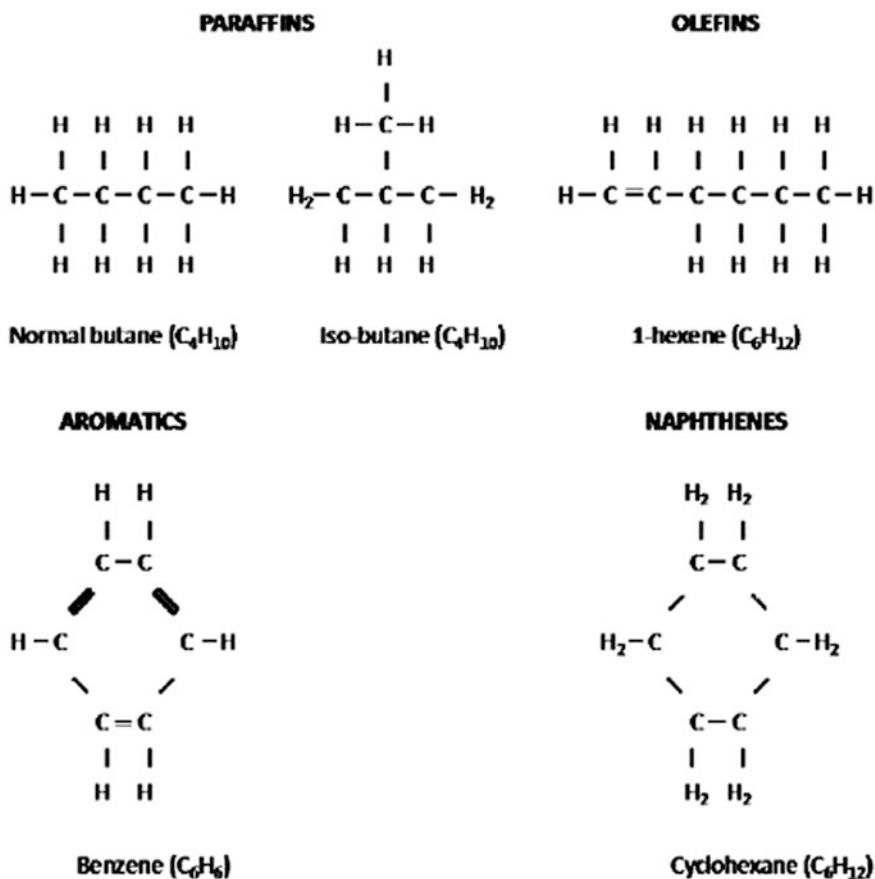


Fig. 2.14 Important classes of hydrocarbon compounds in crude petroleum

Table 2.4 Petroleum fractions

Sl. no	Petroleum fraction	Boiling range ($^{\circ}C$)	Approximate no. of carbon atoms
1	Petroleum ether	30–70	C_5 – C_7
2	Petrol	40–140	C_5 – C_9
3	Naptha	140–180	C_9 – C_{10}
4	Kerosene	180–250	C_{10} – C_{16}
5	Diesel	250–320	C_{10} – C_{18}

- Existence of differential tax levels among the base fuels, intermediate products, and by-products. The adulterants being taxed lower than the base fuels give monetary benefits when mixed with replacing a proportion of the base fuels.

- Differential pricing mechanism of fuels and adulterants and easy availability of adulterants in the market.
- Lack of monitoring and consumers awareness.
- Lack of transparency and uncontrolled regulations in the production-supply and marketing chain for intermediates and by-products of refineries.
- Nonavailability of mechanism and instruments for spot-checking the quality of fuels.

2.6.1.2 Impacts Due to Petroleum Adulteration

High sulfur contents of the kerosene can deactivate the catalyst and lower conversion of engine out pollutants. Kerosene addition may also cause fall in octane quality, which can lead to engine knocking. When petrol is adulterated with diesel fuels, the same effect occurs but usually at lower levels of added diesel fuel. Both diesel and kerosene added to petrol increases engine deposit formation. Petrol may also be adulterated with petrol boiling range solvent such as toluene, xylene, and other aromatics. With the ‘judicious’ adulteration, the petrol would not exhibit drivability problems in motor vehicles. Larger amounts of toluene and/or mixed with xylene cause some increase in HC, CO, NO_x emissions, and significant increase in the level of air toxins—especially benzene—in the tailpipe exhaust. The adulterated petrol itself could have increased potential human toxicity if frequent skin contact is allowed. Extremely high levels of toluene (45 % or higher) could cause premature failure of neoprene, styrene butadiene rubber, and butyl rubber components in the fuel system [112]. This has caused vehicle fires in some cases, especially in older vehicles. Adulteration of gasoline by waste industrial solvents is especially problematic as the adulterants are so varied in composition. They cause increased emissions and may even cause vehicle breakdown. Even low levels of these adulterants can be injurious and costly to vehicle operation. For petrol, any adulterant that changes its volatility can affect drivability. High volatility (resulting from addition of light hydrocarbons) in hot weathers can cause vapor lock and stalling. Low volatility in cold weather can cause starting problems and poor warm-up [113].

The amalgamation of kerosene with automotive diesel is generally practiced by oil industry worldwide as a means of adjusting the low-temperature operability of the fuel. This practice is not harmful or detrimental to tailpipe emissions, provided the resulting fuel continues to meet engine manufacturer’s specifications (especially for viscosity and cetane number). However, high-level adulteration of low sulfur diesel fuel with higher-level sulfur kerosene can cause the fuel to exceed the sulfur maximum. The addition of heavier fuel oils to diesel is usually easy to detect because the resultant fuel will be darker than normal. Depending on the nature of these heavier fuel oils and the possible presence of additional PAHs, there could be some increase in both exhaust PM and PAH emissions.

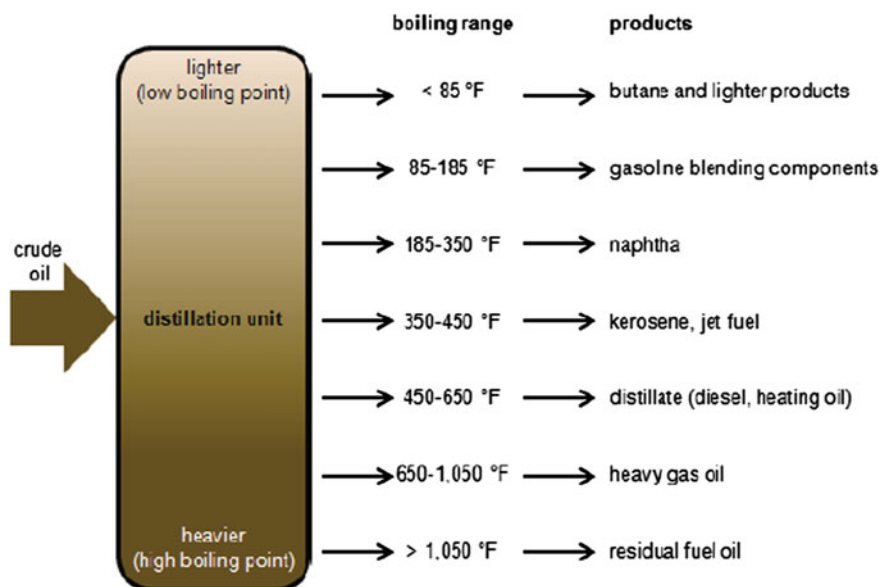


Fig. 2.15 Fractional distillation process: step-by-step

2.6.1.3 Status of Petroleum Adulteration in Indian Context

As mentioned earlier, adulteration of transport fuels at the point of sale and during transportation is a routine problem in India. There are several petroleum products available in our country, which are close substitute of petrol and diesel, but are available at considerable lower prices. The price differential is usually in the range of Rs. 70–80 in the case of petrol and Rs. 50–60 in the case of diesel. Since kerosene is usually considered as poor man's fuel, Govt. of India has been subsidizing it for public distribution for several years. It is common knowledge that significant portion of this subsidized kerosene is being diverted for adulterating petrol. Several studies/survey carried out recently have simultaneously pointed out alarming rise in the cases of fuel adulteration in our country and some of them are as below

- Tata Consultancy has conducted an extensive survey on the kerosene distribution pattern within the country [114]. They arrived at the conclusion that more than 30 % of kerosene distribution intended for household consumption through PDS outlets flowed back to industry in one form or the other. This was a clear indication toward the flourishing business of adulteration in our country.
- According to Antiadulteration Cell of India, Naphtha is a commonly used adulterant for petrol. The modus operandi is to import the product in huge quantity and divert it for adulteration. In a major seizure, recently the Cell detected import of naphtha through the Mangalore Port allegedly for

adulteration of auto-fuels in Kerala, Andhra Pradesh, Karnataka, W. Bengal, and M.P [114]. The intention was to import and move the products to a factory in Pondicherry, where it got blended with other adulterant chemicals. Following the investigation, the Cell sealed 82 kL of naphtha, 31 kL of other products along with plant, and machinery allegedly used for adulteration.

- Similarly a case of adulteration has also been reported from Uttar Pradesh in the city of Meerut, where an authorized transport company was caught with adulterated stock. This transport agency had the authority to transport both petrol and diesel to retail outlets and solvents for industrial use. The agency was supposedly using its workplace for adulterating diesel with kerosene.
- According to news in 'The Times of India,' the State Government of Maharashtra loses a whopping Rs. 81 lakh and Rs. 75.6 lakh every month on account of combined sales and excise tax revenue against petrol and diesel adulteration in Mumbai city alone. This is believed to be 10 % of the genuine sale, industry source reveal [114].
- Various estimates have been made of the extent of financial loss to the national exchequer as well as the oil companies as a result of diversion of PDS kerosene, use of off-spec, low value, hydrocarbons mixed with petrol and diesel, evasion of sales tax, etc. Although these estimates vary over a wide range, it is safe to assume that the nation is losing at least Rs. 10,000 crores annually as a result of adulteration of fuel. If too this is added the social costs as a result of environmental pollution, damage to vehicles and other engines, etc., the loss could be substantially higher [114].
- With the plethora of foreign car manufacturers making a beeline to set up manufacturing facilities in the country, their first and immediate concern is the quality of petrol that gets supplied to the users' cars. They have uniformly found that supplies are heavily adulterated and particularly the octane content is much lower than the specification value of 87 %.
- Recently under the direction of the Supreme Court, Environment Pollution Control Authority (EPCA) through a local NGO (CSE) carried out tests of fuel samples from retail outlets and other points. The results of the study reveal 8.3 % sample failure of the sample tested against 1–2 % reported by oil companies in the past. The study further reveals that adulterated fuel in intelligent mix allowed retail outlets to reap a huge profit of more than Rs. 25,000 a day [114].

2.6.1.4 Petroleum Adulteration Detection as Reported by Earlier Authors

Studies on petrol adulteration started in 1966 with the use of semi-microchromatography to deal with the problem of adulteration [115]. It has the objective of providing an alternative experimental procedure for a modified phase-titration method [116, 117] which shows major improvements over currently

available approaches and has considerable potential as the basis of an ‘in the field’ method of analysis. Table 2.3 shows the previous reported studies on petroleum adulteration detection. Of the range of optical fiber sensors reported in the literature, it is found that the intensity-based optical fiber sensors represent one of the most basic types of optical fiber sensor [118]. But the main drawback of these types of sensors is that the source fluctuations will affect the output intensity which can be overcome using a reference signal. Languease [119] presented an optical fiber refractometer for liquids which eliminates the influence of attenuation due to the liquids. Wiedemann et al. [120] propose a method to detect adulteration by using physico-chemical properties of gasoline samples and performing statistical analysis. Sukhdev Roy [119] proposes a method of changing the refractive index of cladding of fiber for detecting adulteration of fuel which is based on the modulation of intensity of light guided in the fiber due to change in the refractive index of the cladding formed by adulterated fuel and the phenomenon of evanescent wave absorption. Bali et al. [121] has developed an optical sensor for determining the proportional composition of two liquids in a mixture. It is based on changes in the reflected light intensity at the glass–mixture interface brought about by the changes in the proportion of one liquid over that of the other in the mixture. It uses a simple configuration consisting of the end-separated fibers where T–R coupling is decided by medium filled in the gap. This configuration, however, is difficult to handle because of precision needed for alignment so as to get maximum sensitivity.

From the studies mentioned in Table 2.3, it is evident that the optical sensors used in these structures have lesser sensitivity, because of having less sensing area. Moreover, these sensors require more sample volumes for testing. So, these sensors are not suitable for online testing. The planar waveguide sensors proposed in this book (as mentioned in Chap. 4) have more sensitivity requiring less sample volumes for its adulteration detection. In Chap. 5, we have tried to mention how our proposed sensors were used for adulteration sensing with high sensitivity and minimal sample volumes.

2.6.2 Integrated Optical Waveguide Sensor as Detection Element for Laboratory on a Chip-Sensing Application

Since our proposed work contains sensing of glucose concentration in blood, in this context we have tried to report previous works as reported by earlier authors on diagnose/detection of glucose concentration in blood. While significant advances have been made in the incorporation of light sources and detectors into chip-based optical platforms, this section primarily focuses on integrated optical detection with microfluidic Lab on a Chip (LOC) device platform. For separation and concentration of the different components in whole blood, we have seen that microfluidics-based LOC devices use numerous techniques such as acoustophoresis

[126], cross-flow filtration [127], centrifugal forces [128], or gravitational sedimentation [129]. It is seen that LOC offers great possibilities in such applications as clinical point-of-care diagnostics, such as detection of blood glucose concentration, largely due to the fact that they do not involve any complexity. Great advantages include reduction of the analytical testing cost and time and also reduced consumption of sample and reagents. An accurate and fast detection is achievable with LOC, because detection is carried out off-chip which can manipulate small volumes of liquid in microfluidic channels of tens to hundreds of micrometers. This entails the miniaturization of analytical systems and reduction of required sample and reagent volumes onto a small microchip. Although several detection methods are being investigated including optical, magnetic, capacitive, and electrochemical, among these methods, integrated waveguide-based technique using LOC is incredibly advantageous compared to the existing techniques. In such techniques, it is seen that since the governing physics of waveguide operation and the concept of their utility as an analytical device are quite simple, light is guided through the device on account of Frustrated Total Internal Reflection (FTIR), which generates an evanescent optical field that decays exponentially from the sensor surface. The present survey in this section through the relevant literature serves to highlight the most recent progress in applying chip-integrated waveguides for Lab on a Chip (LOC) sensing applications, with special emphasis on detection of glucose level concentration in diabetes.

Development of the LOC technologies offers other indispensable benefits including better process control and lower manufacturing cost [130–132]. It is observed optical sensors using LOC offer compact alternatives to classical instrumentation while delivering comparable performance and disposable formats and makes LOC a superior candidate to support sensing applications. The two main factors that play a character in the choice of detection method for an LOC application are sensitivity and scalability to smaller dimensions. Moreover, devices incorporating LOC do not require a large amount of peripheral equipment for acquisition of detector signal. This makes the development of portable instrumentation based on LOC devices a realistic possibility.

The most important benefits of such an integrated waveguide-based LOC platform include the following:

- Disposability
- Rapid prototyping and a final product with the same tools and materials
- High-process repeatability
- Integrated functionality
- Enabling fabrication of multiple chips simultaneously.

2.6.2.1 Noninvasive Sensing Approach for Measurement of Glucose Concentration

The development of ultra-compact and sensitive sensing structures with minimal sample requirement for accurate sensing has been of great recent interest. Waveguide-based optical sensing technology appears to be exceptionally amenable to chip integration and miniaturization. One of the main advantages of such technology is the possibility to integrate all the functions (chemical, optical, microfluidics, and electronics) in one single platform offering an ideal solution for the implementation of true lab on a chip devices. Figure 2.16 shows an outline of feasible techniques for in vivo glucose measurements and distinguishes invasive, minimal invasive, and noninvasive approaches. Optical techniques such as polarimetry [133, 134], Raman spectroscopy [135, 136], diffuse reflection spectroscopy [137, 138], absorption spectroscopy [139–141], thermal emission spectroscopy [142, 143], fluorescence spectroscopy [144, 145], and photoacoustic (PA) spectroscopy [146–148] have been used to sense glucose with respect to noninvasive monitoring. As we see that most current devices are simple planar devices that do not incorporate the detection and after the reaction has taken place, the readout must be done with complex instrumentation in laboratory settings. That is the main reason why we have incorporated ‘on-chip’ detection by using optical waveguide-based sensors. By using this advanced technology, diagnosis in developing countries for detection of glucose concentration of diabetes patient could become an important achievement for the near future.

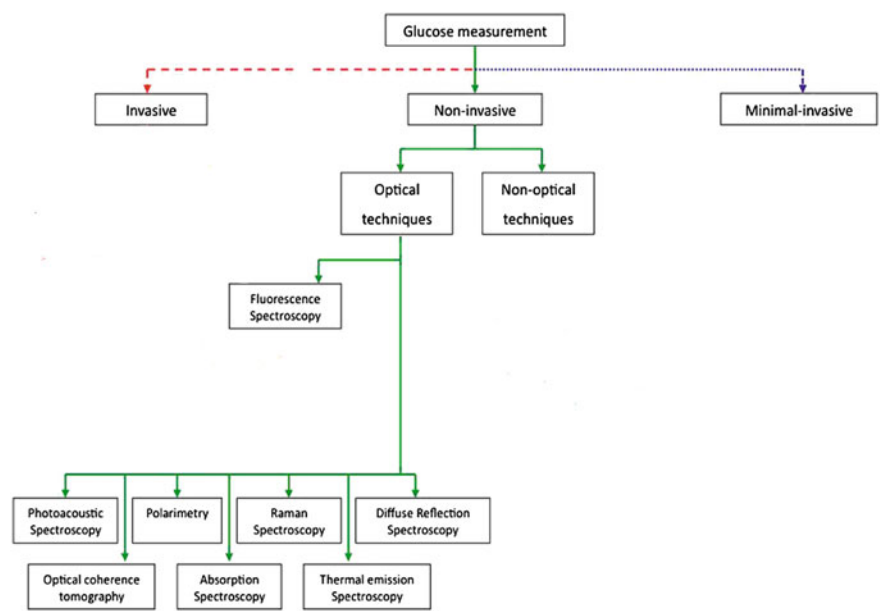
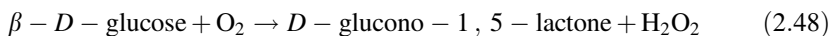
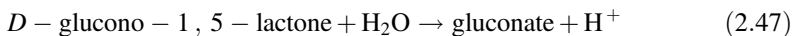


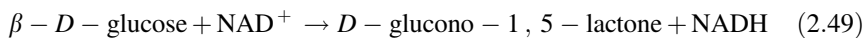
Fig. 2.16 Outline of feasible techniques for in vivo glucose measurements

2.6.2.2 Significance of Sensing Glucose

Although numerous schemes have been developed for the determination of glucose, optical sensors for sensing of glucose are a matter of highly active research. The first sensing schemes for true online sensing (both electrochemical and optical) have been reported several decades ago. One is based on the measurement of the quantity of oxygen consumed according to Eq. (2.47) that is catalyzed by GOx. Alternatively, the H_2O_2 formed according to Eq. (2.47) may be determined by electrochemical or optical means. A third option consists in the determination of the quantity of protons formed (i.e., the decrease in pH) (Eq. 2.48).



The enzyme glucose dehydrogenase also has been used to sense glucose. It catalyzes the conversion of glucose to form a gluconolactone according to Eq. (2.49):



The amount of NADH formed according to Eq. (2.49) may be measured, for example, by photometry at 345 nm or via its fluorescence peaking at 455 nm, but this reaction cannot be easily reversed and comes to an end once all NAD^+ is consumed. Hence, it is less suited (and less elegant) in terms of continuous sensing. The electrons transferred in Eq. (2.47) can be directly shuttled onto an electrode by the so-called direct enzyme wiring (a direct electron transfer from an electrode to the reaction center, either by mediators or by incorporating nano-wires directly into the enzyme) [149, 150]. Sensors employing mediators are in widespread use ever since the 1990s, and sensors based on nano-wires since the year 2000.

All present-day commercial optical sensors rely on the use of GOx. Representative (larger) manufacturers include OptiMedical Inc., Idexx Inc. Becton-Dickinson Comp. Teruma Inc.

2.6.2.3 Glucose Concentration in Human Physiological Fluids—Blood

Monitoring of glucose concentrations (GC) in blood or interstitial fluid is crucial toward understanding the physiological state.

In the quest to demonstrate the benefits of glucose monitoring, several sensors have recently been developed which allow continuous glucose monitoring for several days [151]. The most advanced sensors include the Medtronic Minimed CGMS[®] Gold System[®] from Medtronic Diabetes (Northridge, CA), the STS[®] sensor from DexCom (San Diego, CA) and the FreeStyle Navigator[®] Continuous Glucose Monitor by Therasense/Abbott Diabetes Care (Alameda, CA). These commercially available implantable sensors are based on electroenzymatic sensing

platforms, which exhibit excellent analytical performance *in vitro*. However, they also require a permanent connection from the implanted sensor to an instrument outside the body, providing a potential infection pathway [152], and have drawbacks of instability of the enzyme [153] electrochemical system, inaccuracy, low precision, extended warm-up period, and frequent calibration requirements that make them more cumbersome for *in vivo* use [154–157]. Therefore, most diabetes patients still prefer to measure their blood glucose using a glucometer [158], which involves pain. In fact, the poor patient compliance with recommended testing regimens due to the invasive nature of ‘finger-pricking,’ has further fueled the research for noninvasive and minimally invasive technologies.

Several embodiments of potentially implantable probes have been demonstrated in the past, including enzymatic assays [159–164]. The design and implementation of enzymatic sensors for long term *in vivo* application is complicated due to the consumption of glucose and oxygen, generation of potentially toxic by-products (gluconic acid, hydrogen peroxide), enzyme degradation, and the strong dependence of the glucose response on local tissue oxygen. Therefore, an alternative mechanism based on affinity binding is being investigated by many groups [165–171]. The first affinity-based sensor proposed for monitoring glucose levels within the interstitial fluid was reported by Schultz et al [166]. Since that pioneering effort, a number of advancements toward *in vivo* use have been reported, including poly (ethylene glycol) (PEG) hydrogel microspheres [172] and fuzzy microshells [171]. Follow-up work has extended the optical interactions into the near infrared by labeling Con A and dextran with NIR dyes [170, 173, 174]. However, the true potential for use *in vivo* remains a question because of lingering concerns about Con A toxicity, aggregation, and irreversible binding [175]. For this reason, alternative receptors have been studied for ‘smart tattoo’ formats, including boronic acid derivatives [176–178], apo-enzymes [179–183], and genetically engineered glucose-binding proteins [184, 185]. So, it is found that measurement of glucose concentration in human physiological fluids is of great importance. In clinical diagnosis of metabolic disorders such as diabetes, this is characterized by high levels of glucose in human physiological fluids.

To address these issues, we report on Chap. 6 of this book, development of a technique for rapid detection of glucose concentration in blood plasma using optical waveguide sensor and integrated with LOC. The microfluidic LOC device that we use is a commercially available microfluidic chip (*Product code: 15-1503-0168-02, microfluidic ChipShop GmbH, Stockholmer Str.20D-07747 Jena, Germany, dated: 05-03-2013*) of size 75.5 mm × 25.5 mm × 1.5 mm) [186]. The chip is specifically engineered and optimized for the generation of high-quality plasma. It consists of chamber volume of 25 μL , a luer interface for blood loading, a support channel with a cross section of 300 μm × 100 μm for the transfer of the blood on top of a separation membrane. The ultimate goal of the work of this book was to integrate an entire optical sensing system with LOC for separation of blood plasma from whole blood which is discussed in detail in Chap. 6 of this book.

2.6.2.4 Challenges of Glucose Sensors and Motivation of Planar Waveguide Sensor with Lab on a Chip for Glucose Concentration Measurement

Major advances have been made to enhance functionality of measuring devices for glucose level detection. Despite the impressive advances, it is seen that there are still many challenges related to the achievement of stable and reliable glycemic monitoring. Desirable features of such a sensor system are accuracy, reliability, ultra-sensitivity, fast response, and of course low cost per test. Further, it is very much important that the sensor system is user-friendly and give very accurate results with high sensitivity with very minimal sample. This is one of the reasons that drive the thirst toward the development of integrated devices.

In US patent 6,497,845 [187] issued on behalf of Roche, in December of 2002, an invention is described including a storage container for holding analytical devices (an integrated device). This invention became a commercial product after a couple of years with the launch of Accu-Chek Compact Plus. This device is a blood glucose-monitoring system based on reflectometric technology. The system consists of a meter and dry reagent test strips designed for capillary blood glucose testing by people with diabetes or by healthcare professionals. Compact Plus uses drums with 17 test strips, and the meter is automatically calibrated by inserting a new drum. An electronic check is performed automatically and a test strip is pushed forward when the meter is turned on with a button. The system requires a blood volume of 1.5 μL and provides a result within 5 s. The test principle of Compact Plus relies on the reaction of glucose oxidase with pyrroloquinolone quinone (PQQ). An indicator changes from yellow to blue by means of a mediator and a redox process. The blue color is read reflectometrically. The meter has the capacity to store 300 results in memory. Accu-Chek Softclix Plus lancet pen is fastened to the Compact Plus meter. The lancet pen can be used either when fastened to the meter or it can be taken off the meter.

A method and apparatus for handling multiple sensors in a glucose-monitoring instrument system is described in US patent 5,510,266 [188] issued in April of 1996, in favor of Bayer. The invention is generally related to a glucose-monitoring system and, more particularly, to an improved device for handling multiple sensors that are used in analyzing blood glucose. This invention became a reality in 2003, with the launch of Ascensia Dex, which was the first blood glucose monitor to store multiple strips inside the meter. This device was very easy to use and its integration reduced incorrect results due to the human error. The integration of the test strips in the device was a major innovation, resulting in significant profit to the companies. This is one of the reasons that these patents became a subject of litigation between Roche and Bayer, since there is an apparent similarity between the drum and the disk that Accu-Chek Compact and Ascensia Dex have.

Another challenge that glucose sensor manufacturers had to face is the many manual operating steps in conventional lancet systems (lancet and lancing device),

which is obviously disadvantageous to the user. In most of the systems that are available at present, the lancets for use in lancing devices are provided in a loose form and for each lancing process, the user manually removes a lancet from a pack and has to insert it into the lancet holder of the lancing device and fix it there. Numerous attempts to eliminate the above disadvantage have been described. In US patent 6,616,616 [189], issued in September 2003, Roche describes an invention concerning a lancet system comprising a plurality of essentially needle-shaped lancets, a drive unit which has a drive element in order to move the lancet from the resting position into the lancing position, a storage area to store the lancets, a withdrawal area to guide at least the tip of the lancet out of the system during the lancing process and a transport unit which can transport lancets from the storage area into the withdrawal area. The above invention became a reality in 2004, with the launch of the MultiClix. MultiClix is now one of the most popular lancing devices. It is the only one with a six-lancet drum, combining safety and convenience, since no handling of lancets is necessary. It also provides 11 penetration depth settings, letting the patient adjust the penetration according to his skin type, reducing by this way the pain by avoiding contact with deeper nerves.

Online monitoring of glucose level in diabetes management is certainly a major challenge in the field of clinical diagnostics. In this respect, researchers have demonstrated many techniques for glucose level detection. At the same time, it is seen that nowadays commercial blood glucose meters are also produced by many companies worldwide and the major players are Roche Diagnostics, LifeScan, Abbott, and Bayer who mostly employ mediated amperometric biosensor technology. Other alternative include minimally invasive testing meters and continuous glucose monitoring. We see that as this field enters the area of intense research, the huge demand is creating the need for the development of new approaches with enhanced sensitivity. The trend toward the development of a sensor system with high sensitivity is expected to greatly improve the control and management of diabetes in the very near future. For accurate rapid online measurement of glucose concentration from blood plasma, it requires the following:

- High sensitivity
- Minimal sample volume
- Accurate/online separation of blood plasma
- Low response time sensor
- Use of low-cost material for fabrication of planar waveguide sensor
- Use of conventional IC process technology for fabrication in order to mass production

Keeping all these requirements in mind, we have tried to use our proposed planar waveguide sensor (as mentioned in Chap. 4) for rapid measurement of glucose concentration from blood plasma (which can be transferred to waveguide sensor with capillary pressure obtained for lab on a chip) and reported in Chap. 6.

2.7 Conclusion

In this chapter, a review study on optical sensors that use light to convert bio/chemical processes into a detectable signal has been done as demonstrated by different authors. We have shown how sensitivity is related to the limit of detection (LOD), which is defined as the minimum amount of concentration or mass of the biochemical substance that can be detected by the sensor over the background signal. A mathematical description of wave propagation in planar waveguide using Maxwell's equation has been made to explain evanescent wave sensing phenomenon. For finding the propagation constant, a brief review on different numerical methods such as simple effective index method (SEIM), finite element method (FEM), finite difference time domain (FDTD) method, and beam propagation method (BPM) has also been done. Since SiO_2/SiON has been used as the waveguide material for fabricating the optical sensor, in this context a comparative study also has been done with other waveguide material such as SOI, $\text{SiO}_2/\text{SiO}_2\text{-GeO}_2$, Ti: LiNbO_3 , GaAsInP/InP , and polymeric materials. From the relevant literature survey done in this chapter, it is found that optical sensors based on planar waveguide platform offer the viable advantage of the better control of light path by the use of the optical waveguides and a reduced size with high sensitivity compared to the conventional existing sensors. So, it is required to use optical waveguide sensors with larger sensing area and requirement of minimal sample volume and detection time. We have tried to propose and use waveguide sensors with the above characteristics for application of adulteration of petroleum products and glucose level detection in blood plasma.

References

1. Lifante G (2003) Integrated photonics: fundamentals. Wiley, England
2. Lifante G et al (1997) Planar optical waveguides fabricated by molecular beam epitaxy of Pd-Doped CaF_2 layers. *Appl Phys Lett* 70:2079–2081
3. Stoffer R et al (2000) Numerical studies of 2D photonic crystals: waveguides, coupling between waveguides and filters. *Opt Quantum Electron* 32(6–8):947–961
4. Snyder AW, Love JD (1983) Optical waveguide theory. Chapman & Hall, London and New York
5. Marz R (1995) Integrated optics: design and modeling. Artech House, Norwood
6. Marcatili EAJ (1969) Dielectric rectangular waveguide and directional coupler for integrated optics. *Bell Syst Tech J* 48(i7):2071–2102
7. Knox RM, Toullos PP (1970) Integrated circuits for the millimeter through optical frequency range. Paper presented at the submillimeter waves international symposium, Brooklyn, 31 March–2 April, New York
8. Nishihara H, Haruna M, Suhara T (1989) Optical integrated circuits. McGraw-Hill, New York

9. Rahman BAM, Davies JB (1983) Finite element analysis of optical and microwave problems. *IEEE Trans Microwave Theory Tech* MTT 32(1):20–28
10. Koshiba M et al (1985) Improved finite element formulation in terms of the magnetic fields vector for dielectric waveguides. *IEEE Trans Microwave Theory Tech* MTT 33(3):227–233
11. Lee JF et al (1991) Full wave analysis of dielectric waveguides using tangential finite elements. *IEEE Trans Microwave Theory Tech* MTT 39(8):1262–1271
12. Yee KS (1966) Numerical solution of initial boundary value problems involving Maxwell's equations in isotropic media. *IEEE Trans Antennas Propag AR* 14(3):302–307
13. Taflov A (1995) Computational electrodynamics: the finite difference time domain method. Artech House, Norwood
14. Ridder RM et al (1998) Silicon oxynitride planar waveguiding structures for application in optical communication. *IEEE J Sel Top Quantum Electron* 4(6):930–937
15. Strang G (1968) On the construction and comparison of difference schemes. *SIAM J Numer Anal* 5(3):506–517
16. Shang JS (1995) Characteristic based methods for the time-domain Maxwell equations. *IEEE Antennas Propag Mag* 37(3):15–25
17. Colella P, Woodward PR (1984) The piecewise parabolic method (PPM) for gas dynamical simulations. *J Comp Phys* 54(1):174–201
18. Hadley GR (1992) Transparent boundary condition for the beam propagation method. *J Quantum Electron* 28(1):363–370
19. Feng N (2005) An efficient split-step time-domain beam-propagation method for modeling of optical waveguide devices. *J Lightwave Technol* 23(6):2186–2191
20. Manoharan K (2009) Design and analysis of high-Q, amorphous micro ring resonator sensor for gaseous and biological species detection, M.S. Thesis, University of Ohio at Athens, USA
21. Fossum ER (1997) CMOS image sensors: electronic camera-on-a-chip. *IEEE Trans Electron Dev* 44(10):1689–1698
22. Passaro VMN et al (2006) Review electromagnetic field photonic sensors. *Prog Quantum Electron* 30(2–3):45–47
23. Krioukov E et al (2002) Integrated optical microcavities for enhanced evanescent-wave spectroscopy. *Opt Lett* 27(17):1504–1506
24. Campopiano S et al (2004) Microfluidic sensor based on integrated optical hollow waveguides. *Opt Lett* 29(16):1894–1896
25. Zhang AP (2012) Advances in optical fiber Bragg grating sensor technologies. *Photonic Sens* 2(1):1–13
26. Passaro VMN, Dell'olio F (2007) Guided-wave optical biosensors. *Sensors* 7(4):508–536
27. Yu FTS, Shizhuo Y (2002) Fiber optic sensors. Marcel Decker Inc, New York
28. Inaudi D, Glisic B (2008) Overview of fibre optic sensing applications to structural health monitoring. Paper presented at the symposium on deformation measurement and analysis Lisbon, Portugal, 12–15 May 2008
29. Fidanboyli K, Efendioglu H S (2009) Fiber Optic Sensors and Their Applications. In: Proceedings of 5th international advanced technologies symposium, Karabuk University, Turkey, 13–15 May 2009
30. Yin SZ, Ruffin PB, Yu FTS (2008) Fiber optic sensors. CRC Press, Taylor & Francis Group, Boca Raton
31. Xiangyang L et al (2012) Fiber-optical sensors: basics and applications in multiphase reactors. *Sensors* 12(9):12519–12544
32. Méndez A (2013) Overview of fiber optic sensors for NDT applications in nondestructive testing of materials and structures. Springer, New York
33. Jenny R (2000) Fundamentals of fiber optics: an introduction for beginners. Volpi Manufacturing USA Co, New York

34. Casas JR, Paulo JS (2003) Fiber optic sensors for bridge monitoring. *J Bridge Eng* 8(6):362–373
35. Berthold JW (1995) Historical review of microbend fiber optic sensors. *J Lightwave Technol* 13(7):1193–1199
36. Hauptmann P (1993) *Sensors: principles and applications*. Prentice Hall, Englewood Cliffs
37. Krohn DA (1988) *Fiber optic sensors: fundamental and applications*. Instrument Society of America, Research Triangle Park, North Carolina
38. Johnson LM et al (1982) Integrated optical temperature sensor. *Appl Phys Lett* 41(2):134–136
39. Izutsu M et al (1983) Optical-waveguide micro-displacement sensor. *Elect Lett* 18(20):867–868
40. Kersten RT (1988) *Integrated optics for sensors*. Opt Fiber Sensors. Artech House, Norwood
41. Parriaux O (1994) *Integrated optics sensors*. In: Martellucci S, Chester AN, Bertolotti M (eds) *Advances in integrated optics*. Springer, Plenum Press, New York
42. Luff BJ et al (1998) Integrated optical Mach-Zehnder biosensor. *J Light Technol* 16(4):583–592
43. Jimenez D et al (1996) An integrated silicon ARROW Mach-Zehnder interferometer for sensing applications. *Opt Commun* 132(5–6):437–441
44. Righini GC, Tajani A, Cutolo A (2009) *An introduction to optoelectro sensors*. World Scientific Publishing, Singapore
45. Hunsperger RG (1982) *Integrated optics: theory and technology*. Springer Verlag, Berlin
46. Lukosz W et al (1991) Input and output grating couplers as integrated optical biosensors. *Sens Actuators A* 25(1–3):181–184
47. Grattan KTV, Meggitt BT (1999) *Optical fiber sensor technology*. Kluwer academic publishers, Netherlands
48. Baldini F et al (2006) *Optical chemical sensors*. Springer, Netherlands
49. Sanchis P et al (2007) Design of silicon-based slot waveguide configurations for optimum nonlinear performance. *J Lightwave Technol* 25(5):1298–1305
50. Pandraud G et al (2000) Evanescent wave sensing: new features for detection I small volumes. *Sens Actuators A Phys* 85(1–3):158–162
51. Kumar PS et al (2002) A fibre optic evanescent wave sensor used for the detection of trace nitrites in water. *J Opt A Pure Appl Opt* 4(3):247–250
52. Helmers H et al (1996) Performance of a compact, hybrid optical evanescent-wave sensor for chemical and biological applications. *Appl Opt* 35(4):676–680
53. Kasap SO (2001) *Optoelectronics and photonics*. Prentice Hall, Canada
54. Lukosz W (1995) Integrated optical chemical and direct biochemical sensors. *Sens Actuators B* 29(1–3):37–50
55. Lambeck PV et al (2006) Three novel integrated optical sensing structures for the chemical domain. *Sens Actuators B* 113(2):718–729
56. Homola J et al (1999) Surface plasmon resonance sensors: review. *Sens Actuators B* 54(1–2):3–15
57. Kretschmann E (1971) Die Bestimmung optischer Konstanten von Metallen durch Anregung von Oberflächenplasmaschwingungen. *Physik* 241(4):313–324
58. Nylander C et al (1982) Gas detection by means of surface plasmon resonance. *Sens Actuators* 3:79–88
59. Liedberg B et al (1983) Surface plasmon resonance for gas detection and biosensing. *Sens Actuators* 4:299–304
60. Sheridan AK et al (2004) Phase interrogation of an integrated optical SPR sensor. *Sens Actuators B* 97(1):114–121
61. Homola J (2006) *Surface plasmon resonance based sensors*. Springer, Prague, Czech Republic

62. Lukosz W, Tiefenthaler K (1998) Sensitivity of integrated optical grating and prism couplers as (bio)chemical sensors. *Sens Actuators* 15(3):273–284
63. Lukosz W, Tiefenthaler K (1989) Sensitivity of grating couplers as integrated optical chemical sensors. *J Opt Soc Am B* 6(2):209–220
64. Lukosz W (1991) Principles and sensitivities of integrated optical and surface plasmon sensors for direct affinity and immunosensing. *Biosens Bioelectron* 6(3):215–225
65. Lukosz W, Tiefenthaler K (1983) Embossing technique for fabricating integrated optical components in hard inorganic wave guiding materials. *Opt Lett* 8(10):537–539
66. Heuberger K, Lukosz W (1986) Embossing technique for fabricating surface relief gratings on hard oxide waveguides. *Appl Opt* 25(9):1499–1504
67. Lukosz W, Tiefenthaler K (1983) Directional switching in planar waveguides effected by adsorption desorption processes. Paper presented at the 2nd European conference integrated optics florence, 17–18 Oct 1983
68. Tiefenthaler K, Lukosz W (1984) Integrated optical humidity and gas sensors. Germany, date month, Paper presented at the Intl Conf on Optical Fiber Sensors, Stuttgart
69. Tiefenthaler K, Lukosz W (1985) Grating couplers as integrated optical humidity and gas sensors. *Thin Solid Films* 126(3–4):205–211
70. Tiet’enthaler K (1985) Embossed surface-relief gratings on planar waveguides as integrated optical switches and gas sensors, Ph.D. Thesis, University of ETH Zurich at Zurich
71. Burke CS et al (2006) Development of an optical sensor probe for the detection of dissolved carbon dioxide. *Sens Actuators B Chem* 119(1):288–294
72. Burke CS et al (2006) Planar optical sensors and evanescent wave effects. *Opt Chem Sens*. Springer, Netherlands, pp 193–215
73. Brandenburg A et al (1995) Ammonia detection via integrated optical evanescent wave sensors. *Mikrochim Acta* 121:95–105
74. Pandraud G et al (2000) Evanescent wave sensing: new features for detection in small volumes. *Sens Actuators* 85(1–3):158–162
75. Cunningham BT (2007) Label-free optical biosensors: an introduction in label-free biosensors: techniques and applications. Cambridge University Press, Cambridge, pp 1–28
76. D’Amico A, Natale CD (2001) A contribution on some definitions of sensors properties. *IEEE Sens J* 1(3):183–190
77. Deka B (2013) Ph. D. Thesis, Tezpur University
78. Wörhoff K et al (2002) Silicon oxynitride-a versatile material for integrated optics applications. *J Electrocheml Soc* 149(8):F85–F91
79. Offrein BJ et al (1999) Wavelength tunable optical add after drop filter with flat pass band for WDM networks. *IEEE Photonics Tech Lett* 11(2):239–241
80. Janz F et al (1995) Bent waveguide couplers for demultiplexing of arbitrary broadly separated wavelengths using two mode interference. *IEEE Photonics Tech Lett* 7 (9):1037–1039
81. Zappe HP, Neyer A (1984) Integrated optical multichannel wavelength multiplexer for monomode system. *IEEE Electron Lett* 20:744–746
82. Papuchon M et al (1977) Electrically active optical bifurcation: BOA. *Appl Phys Lett* 31 (4):266–267
83. Zappe HP (1995) Introduction to semiconductor integrated optics. Artech House, Boston
84. Kashahara R et al (2002) New structures of silica-based planar light wave circuits for low power thermo optic switch and its application to 8×8 optical matrix switch. *J Lightwave Technol* 20(6):993–1000
85. Takato N et al (1990) Silica based integrated optic Mach Zehnder multi/demultiplexer family with channel spacing of 0.01–250 nm. *IEEE Sel Areas Comm* 8(6):1120–1127
86. Yagi M et al (2000) Versatile multimodes interference photonic switches with partial index modulation regions. *IEEE Electron Lett* 36(6):533–534

87. Darmawan S et al (2005) A rigorous comparative analysis of directional couplers and multimode interferometers based on ridge waveguides. *IEEE J Sel Top Quantum Electron* 11 (2):466–475
88. Ma Y et al (2000) Ultracompact multimode interference 3-dB coupler with strong lateral confinement by deep dry etching. *IEEE Photonics Lett* 12(5):492–494
89. Leuthold J, Joyner CH (2001) Multimode interference couplers with tunable power splitting ratios. *IEEE J Lightwave Technol* 19(5):700–707
90. Offrein BJ et al (2000) Adaptive gain equalizer in high index contrast SiON technology. *IEEE Photonics Tech Lett* 12(5):504–506
91. Kumar D, Singh V (2011) Theoretical modeling of a nonlinear asymmetric metal-clad planar waveguide based sensors. *Optik* 122(20):1872–1875
92. Parriaux O, Dierauer P (1994) Normalized expressions for the optical sensitivity of evanescent wave sensors: erratum. *Opt Lett* 19(20):1665–1665
93. Taya SA et al (2009) Enhancement of sensitivity in optical waveguide sensors using left-handed materials. *Optik* 120(10):504–508
94. Carlos AB et al (2008) Label-free optical biosensing with slot-waveguides. *Opt Lett* 33 (7):708–710
95. Karasinski P (2009) Planar optical waveguide sensor structures with grating couplers. *Acta Phys Pol A* 116:30–32
96. Carlos AB (2009) Optical slot-waveguide based biochemical sensors. *Sensors* 9(6):4751–4765
97. Densmore A et al (2006) A silicon-on-insulator photonic wire based evanescent field sensor. *IEEE Photonic Tech Lett* 18(23):2520–2522
98. Karasinski P (2011) Optical uniform/gradient waveguide sensor structure characterization. *Opto Electron Rev* 19(1):01–09
99. Sofyan AT, Taher ME (2011) A reverse symmetry optical waveguide sensor using a plasma substrate. *J Opt* 13:1–6
100. Renling Z et al (2010) The sensing structure optimization of planer optical waveguide with fermi refractive index. *J Lightwave Technol* 28(23):3439–3443
101. Yimit A et al (2005) Thin film composite optical waveguides for sensor applications: a review. *Talanta* 65(25):1102–1109
102. Airoudj A et al (2008) Design and sensing properties of an integrated optical gas sensor based on a multilayer structure. *J Anal Chem* 80(23):9188–9194
103. Veldhuis GJ et al (2000) Sensitivity enhancement in evanescent optical waveguide sensors. *J Lightwave Technol* 18(5):677–682
104. Gupta AK, Sharma RK (2010) A new method for estimation of automobile fuel adulteration. In: *Pollution Air* (ed) Sciyo. Croatia, Rijeka, pp 357–370
105. Bhatnagar VP (1981) An ultrasonic method to find liquid fuel adulteration. *J Acoust Soc India* 9:19–23
106. Bahari MS et al (1990) Determination of the adulteration of petrol with kerosene using rapid phase titration procedure. *Anal* 115:417–419
107. Bahari MS et al (1991) Spectrophotometric end-point phase-titration determination of the adulteration of petrol with kerosene. *Anal Proc* 28:14–16
108. Srivastava A et al (1997) Optical sensor for determining adulteration in petrol by kerosene. In *Proceedings of the international conference on fiber optics and photonics*, New Delhi
109. Sharma RK, Gupta AK (2007) Detection/estimation of adulteration in gasoline and diesel using ultrasonics. Paper presented at the international conference on industrial and information systems, Penadeniya, 9–11 Aug 2007
110. Yadav SR et al (2005) Estimation of petrol and diesel adulteration with kerosene and assessment of usefulness of selected automobile fuel quality test parameters. *Intl J Environ Sci Technol* 1(4):253–255

111. Roy S (1999) Fiber optic sensor for determining adulteration of petrol and diesel by kerosene. *Sens Actuators B* 55(2–3):212
112. Osueke Engr CO, Ofondu Engr IO (2011) Fuel adulteration in nigeria and its consequences. *Intl J Mech Mechatr Engg* 11(4):32–35
113. Aziz al RA (2008) Ph. D. Thesis, King Saud University, Riyadh, Kingdom of Saudi Arabia
114. Gawande AP, Kaware JP (2013) Fuel adulteration consequences in India: a review. *Sci Revs Chem Commun* 3(3):161–171
115. Paulo JM et al (2012) A study of adulteration in gasoline samples using flame emission spectroscopy and chemometrics tools. *Anal* 137:5919–5924
116. Tsubochi M et al (1979) Determination of anionic surfactants by two-phase titration with tetrabromophenolphthalein ethyl ester as indicator. *J Am Oil Chemists' Soc* 56(11):921–923
117. Suri SK (1972) Analysis by phase-titration of three-component systems containing two mutually immiscible or partially miscible components. *Talanta* 19(6):804–807
118. Chandy RP et al (2000) An optical fiber sensor for biofilm measurement using intensity modulation and image. *IEEE J Sel Top Quantum Electron* 6(5):764–772
119. Laguesse M (1988) An optical fibre refractometer for liquids using two measurement channels to reject optical attenuation. *J Phys E Sci Instrum* 21(1):64–67
120. Wiedemann LSM et al (2005) Adulteration detection of Brazilian gasoline samples by statistical analysis. *Fuel* 84(4):467–473
121. Bali LM et al (1999) Optical sensor for determining adulteration in a liquid sample. *Opt Eng* 38(10):1715–1721
122. Kishor K et al (2011) Optical sensor for the determination of adulteration in petrol: design and development. In: *Novel optical systems design and optimization XIV* (2011), San Diego, California, USA
123. Bahari MS et al (1991) Spectrophotometric end-point for the phase-titration determination of the adulteration of petrol with kerosene. *Anal Proc* 28:14–16
124. Mishra V et al (2008) Fuel adulteration detection using long period fiber grating sensor technology. *Ind J Pure App Phys* 46(02):106–110
125. Patil SS (2011) Refractometric fiber optic adulteration level detector for diesel. *Int J Adv Engg Technol* 1(4):195–203
126. Lenshof A et al (2009) Acoustic whole blood plasmapheresis chip for prostate specific antigen microarray diagnostics. *Anal Chem* 81(15):6030–6037
127. Tachi T et al (2009) Simultaneous separation, metering, and dilution of plasma from human whole blood in a microfluidic system. *Anal Chem* 81(8):3194–3198
128. Haeberle S et al (2006) Centrifugal extraction of plasma from whole blood on a rotating disk. *Lab Chip* 6:776–781
129. Dimov IK et al (2011) Stand-alone self-powered integrated microfluidic blood analysis system (SIMBAS). *Lab Chip* 11:845–850
130. Whitesides GM (2006) The origins and the future of microfluidics. *Nat* 442:368–373
131. Kuswandi B et al (2007) Optical sensing systems for microfluidic devices: a review. *Anal Chim Acta* 601(2):141–155
132. Mark D et al (2010) Microfluidic lab-on-a-chip platforms: requirements, characteristics and application. *Chem Soc Rev* 39(3):1153–1182
133. Chou C et al (1998) Noninvasive glucose monitoring in vivo with an optical heterodyne polarimeter. *Appl Opt* 37(16):3553–3557
134. Malik BH (2010) Real-time, closed-loop dual-wavelength optical polarimetry for glucose monitoring. *J Biomed Opt* 15(1):017002
135. Enejder AM et al (2005) Raman spectroscopy for noninvasive glucose measurements. *J Biomed Opt* 10(3):031114
136. Lambert JL et al (2005) Glucose determination in human aqueous humor with Raman spectroscopy. *J Biomed Opt* 10(3):031110

137. Marbach R et al (1993) Noninvasive blood glucose assay by near-infrared diffuse reflectance spectroscopy of the human inner lip. *Appl Spectro* 47(7):875–881
138. Maruo K et al (2003) In vivo noninvasive measurement of blood glucose by nearinfrared diffuse-reflectance spectroscopy. *Appl Spectrosc* 57(10):1236–1244
139. Vrancic C et al (2011) Continuous glucose monitoring by means of mid-infrared transmission laser spectroscopy in vitro. *Anal* 136(6):1192–1198
140. Gabriely I et al (1999) Transcutaneous glucose measurement using near-infrared spectroscopy during hypoglycemia. *Diabet Care* 22(12):2026–2032
141. Spanner G, Niessner R (1996) New concept for the non-invasive determination of physiological glucose concentrations using modulated laser diodes. *Fresenius J Anal Chem* 354(3):306–310
142. Malchoff CD et al (2002) A novel noninvasive blood glucose monitor. *Diabet Care* 25:2268–2275
143. Guo X et al (2010) Wavelength-modulated differential laser photothermal radiometry for blood glucose measurements. *J Phys Conf Ser* 214(1):012025
144. Ballerstadt R et al (2006) In vivo performance evaluation of a transdermal near-infrared fluorescence resonance energy transfer affinity sensor for continuous glucose monitoring. *Diabet Technol Ther* 8(3):296–311
145. March W et al (2006) Fluorescent measurement in the non-invasive contact lens glucose sensor. *Diabetes Technol Ther* 8(3):312–317
146. Kottmann J et al (2011) New photoacoustic cell design for studying aqueous solutions and gels. *Rev Sci Instrum* 82:084903
147. Spanner G, Niessner R (1996) Noninvasive determination of blood constituents using an array of modulated laser diodes and a photoacoustic sensor head. *Fresenius J Anal Chem* 355 (3–4):306–310
148. Zhao Z (2002) Ph.D. thesis, University of Oulu
149. Heller A, Feldman B (2008) Electrochemical glucose sensors and their applications in diabetes management. *Chem Rev* 108:2482–2505
150. Tuchin VM (2009) Commercial biosensors for diabetes. In: Fragkou V, Turner APF (eds) *Handbook of optical sensing of glucose in biological fluids and tissues*. CRC press, Boca Raton, Fla, pp 41–64
151. Klonoff DC (2005) Continuous glucose monitoring: roadmap for 21st century diabetes therapy. *Diabet Care* 28(5):1231–1239
152. Skyler JS (2009) Continuous glucose monitoring: an overview of its development. *Diabet Technol Ther* 11(Suppl. 1):S5–S10
153. Valdes TI, Moussy F (2000) In vitro and in vivo degradation of glucose oxidase enzyme used for an implantable glucose biosensor. *Diabet Technol Ther* 2(3):367–376
154. Pickup J (1999) In vivo glucose sensing for diabetes management: progress towards non-invasive monitoring. *BMJ* 319(7220):1289
155. Pickup JC et al (2005) In vivo glucose monitoring: the clinical reality and the promise. *Biosens Bioelectron* 20(10):1897–1902
156. Gerritsen M et al (1999) Performance of subcutaneously implanted glucose sensors for continuous monitoring. *Neth J Med* 54(4):167–179
157. Wickramasinghe Y et al (2004) Current problems and potential techniques in vivo glucose monitoring. *J Fluoresc* 14(5):513–520
158. Newman JD, Turner AP (2005) Home blood glucose biosensors: a commercial perspective. *Biosens Bioelectron* 20(12):2435–2453
159. Brown JQ et al (2005) Encapsulation of glucose oxidase and an oxygen-quenched fluorophore in polyelectrolyte-coated calcium alginate microspheres as optical glucose sensor systems. *Biosens Bioelectron* 21(1):212–216
160. Brown JQ et al (2006) Enzymatic fluorescent microsphere glucose sensors: evaluation of response under dynamic conditions. *Diabetes Technol Ther* 8(3):288–295

161. Zhu H et al (2005) Combined physical and chemical immobilization of glucose oxidase in alginate microspheres improves stability of encapsulation and activity. *Bio Conjug Chem* 16 (6):1451–1458
162. Zhu H, McShane MJ (2005) Macromolecule encapsulation in diazoresin-based hollow polyelectrolyte microcapsules. *Langmuir* 21(1):424–430
163. Zhu H et al (2005) Spontaneous loading of positively charged macromolecules into alginate-templated polyelectrolyte multilayer microcapsules. *Biomacromolec* 6(4):2221–2228
164. Stein EW et al (2007) Microscale enzymatic optical biosensors using mass transport limiting nanofilms. 1. Fabrication and characterization using glucose as a model analyte. *Anal Chem* 79(4):1339–1348
165. Schultz JS, Sims G (1979) Affinity sensors for individual metabolites. *Biotechnol Bioeng Symp* 9:65–71
166. Schultz JS et al (1982) Affinity sensor: a new technique for developing implantable sensors for glucose and other metabolites. *Diabet Care* 5:245–253
167. Meadows DL, Schultz JS (1993) Design, manufacture and characterization of an optical fiber glucose affinity sensor based on an homogeneous fluorescence energy transfer assay system. *Anal Chim Acta* 280:21–30
168. Mansouri S, Schultz JS (1984) A miniature optical glucose sensor based on affinity binding. *Nat Biotechnol* 2:885–890
169. Ballerstadt R, Schultz JS (2000) A fluorescence affinity hollow fiber sensor for continuous transdermal glucose monitoring. *Anal Chem* 72(17):4185–4192
170. Ballerstadt R et al (2004) In vitro long-term performance study of a near-infrared fluorescence affinity sensor for glucose monitoring. *Biosens Bioelectron* 19(8):905–914
171. Chinnayelka S, McShane MJ (2004) Glucose-sensitive nanoassemblies comprising affinity-binding complexes trapped in fuzzy microshells. *J Fluoresc* 14(5):585–595
172. Russell RJ et al (1999) A fluorescence-based glucose biosensor using concanavalin a and dextran encapsulated in a poly (ethylene glycol) hydrogel. *Anal Chem* 71(15):3126–3132
173. Ballerstadt R et al (2004) Fluorescence resonance energy transfer-based near-infrared fluorescence sensor for glucose monitoring. *Diabet Technol Ther* 6(2):191–200
174. Ballerstadt R et al (2006) In vivo performance evaluation of a transdermal near-infrared fluorescence resonance energy transfer affinity sensor for continuous glucose monitoring. *Diabet Technol Ther* 8(3):296–311
175. Ballerstadt R et al (2006) Concanavalin a for in vivo glucose sensing: a biotoxicity review. *Biosens Bioelectron* 22(2):275–284
176. Fang H et al (2004) Progress in boronic acid-based fluorescent glucose sensors. *J Fluoresc* 14 (5):481–489
177. Kawanishi T et al (2004) A study of boronic acid based fluorescent glucose sensors. *J Fluoresc* 14(5):499–512
178. Phillips MD, James TD (2004) Boronic acid based modular fluorescent sensors for glucose. *J Fluoresc* 14(5):549–559
179. Chaudhary A et al (2009) Evaluation of glucose sensitive affinity binding assay entrapped in fluorescent dissolved-core alginate microspheres. *Biotechnol Bioeng* 104(6):1075–1085
180. Chaudhary A, Srivastava R (2008) Glucose sensing using competitive binding assay co-encapsulated in uniform sized alginate microspheres. *Sens Lett* 6(2):253–260
181. Chinnayelka S, McShane MJ (2004) Resonance energy transfer nanobiosensors based on affinity binding between apo-enzyme and its substrate. *Biomacromol* 5(5):1657–1661
182. Chinnayelka S, McShane MJ (2005) Microcapsule biosensors using competitive binding resonance energy transfer assays based on apoenzymes. *Anal Chem* 77(17):5501–5511
183. Chinnayelka S et al (2008) Near-infrared resonance energy transfer glucose biosensors in hybrid microcapsule carriers. *J Sensor* (Article ID 346016):1–10

184. D'Auria S et al (2000) A thermophilic apoglucose dehydrogenase as nonconsuming glucose sensor. *Biochem Biophys Res Commun* 274(3):727–731
185. Tolosa L et al (1999) Glucose sensor for low-cost lifetime-based sensing using a genetically engineered protein. *Anal Biochem* 267(1):114–120
186. Gärtner C Microfluidic ChipShop. http://www.microfluidic-chipshop.eu/Download/Lab-on-a-Chip%20Catalogue_032014.pdf
187. Sacherer, US Patent 6,497,845, 24 December 2002
188. Bonner et al, US Patent 5,510,266, 23 April 1996
189. Fritz et al US Patent 6,616,616, 9 September 2003

Planar Waveguide Optical Sensors

From Theory to Applications

Dutta, A.; Deka, B.; Pratim Sahu, P.

2016, XXV, 179 p. 84 illus., 51 illus. in color., Hardcover

ISBN: 978-3-319-35139-1